ASSEMBLY-SCALE AND WHOLE-BUILDING ENERGY PERFORMANCE ANALYSIS OF ULTRA-HIGH-PERFORMANCE FIBER-REINFORCED CONCRETE (UHP-FRC) FAÇADE SYSTEMS

by

BAHRAM ABEDINIANGERABI

DISSERTATION

Submitted in partial fulfillment of the requirements
for the degree of Doctor of Philosophy at The
University of Texas at Arlington

December 2019

Arlington, Texas

Supervising Committee:

Dr. Mohsen Shahandashti, Supervising Professor

Dr. Shih-Ho Chao

Dr. Mohammad Najafi

Prof. Bradley Bell

Dr. Atefe Makhmalbaf

Dedicated to

My parents, Esmaeil and Touran, and my beloved wife, Shirin, for their endless support, encouragement, patience and unconditional love.

Acknowledgements

I would like to express my most sincere gratitude and appreciation to my academic advisor and mentor, Dr. Mohsen Shahandashti, for his continuous encouragement, invaluable support, endless patience, and excessive interest that made me energetic to continue studying and working hard. I was fortunate to assist Dr. Shahandashti in several research projects over the last four years, and I am indebted for the opportunities he provided me throughout my graduate studies that helped me improve myself both academically and professionally. His insight has significantly assisted me in choosing my career path, presently and in the future.

I would like to thank my committee members, Dr. Shih-Ho Chao, Dr. Mohammad Najafi, Prof. Bradley Bell, and Dr. Atefe Makhmalbaf for their valuable insightful questions, suggestions, great comments, and contributions to my dissertation.

I would like to thank my friends and colleagues at UTA, Ehsan Zahed, Navid Ahmadi, Binaya Pudasaini, Anil Baral, Pouria Pourmand, Ferika Farooghi, Pooya Darghiasi, Mina Zamanian, Wasiq Ameen, Abhijit Roy, and Sooin Kim for all the great discussions and fun we had.

Last but not least, I am grateful to my family specially my mother, my father, and my lovely wife. Without their dedication and love, it would not have been possible for me to achieve this accomplishment.

Abstract

ASSEMBLY-SCALE AND WHOLE-BUILDING ENERGY PERFORMANCE ANALYSIS OF ULTRA-HIGH-PERFORMANCE FIBER-REINFORCED CONCRETE (UHP-FRC) FAÇADE SYSTEMS

Bahram Abediniangerabi

The University of Texas at Arlington, 2019

Supervising Professor: Mohsen Shahandashti

The majority of building energy consumption is used to heat and cool enclosed spaces. An innovative ultra-high-performance fiber-reinforced concrete (UHP-FRC) façade system could potentially reduce this energy consumption by utilizing UHP-FRC's high structural strength and ductility hence more space for insulation. The energy performance assessment of innovative façade systems such as UHP-FRC panels could be misleading if the effect of building types and climate contexts on building energy consumption is not considered. Moreover, thermal bridging and hygrothermal analyses of UHP-FRC panels are needed to investigate the heat and moisture transfer within the panels. The main objectives of this study are (1) analyzing of heat and moisture transfer within the proposed UHP-FRC

façade panel in a detailed assembly scale, (2) investigating the effect of panel connections in the hygrothermal performance of UHP-FRC façade panels, (3) investigating the combined effect of different building types and climate conditions on these panels' energy performance under uncertainty, and (4) identifying and analyzing hidden underlying patterns in simulated data through knowledge discovery and pattern recognition.

A Numerical heat and moisture transfer simulations were conducted to evaluate the amount of thermal bridging and the risk of mold growth within innovative UHP-FRC façade systems. The results of the thermal bridging analysis showed that the UHP-FRC panel provides unique thermal properties with higher thermal resistance compared with the conventional panel assembly. The UHP-FRC panel assembly minimizes the thermal bridging by eliminating the structural rebars.

A transient, coupled heat and moisture transfer analysis was conducted in order to investigate the effect of panel connections in the hygrothermal behavior of facade panels. The results of heat hygrothermal assessment showed that steel connections could significantly reduce the thermal resistivity of façade panels by converging heat fluxes and acting as thermal bridges within façade panels. The results also showed that the steel connector of the panel to foundation connection had ten times higher maximum heat flux compared to the other connections. In addition, the results of moisture transfer showed that air gaps between the panels had higher moisture flux compared to the other layers in the connections. Therefore,

new connection designs and materials are essential for innovative façade systems, such as UHP-FRC panels, to effectively exploit the potential opportunities provided by façade systems.

A probabilistic simulation-based building energy performance analysis was also conducted to investigate the combined effect of different building types and climate conditions on the energy performance of UHP-FRC panel systems. The analysis was conducted for fourteen U.S. Department of Energy prototype buildings in fifteen climate zones (210 scenarios). The results showed that the energy savings of using UHP-FRC panels depend on the building type and climate condition. On average, energy savings are higher in colder climates (e.g., Fairbanks) than those in temperate climates (e.g., San Francisco). Also, buildings dominated by internal loads seem to benefit the least from UHP-FRC.

A data-driven framework was developed to extract hidden information and underlying structure from the thermal behavior of UHP-FRC façade systems in a set of scenarios and provide recommendations for designers to select energy-efficient façade systems. In the proposed framework, clustering analysis was used to partition simulated data into different subsets with distinct patterns. Then, the association rule mining (ARM) technique was applied to each dataset to extract rules as recommendations for positive, negative, and neutral energy savings related to the UHP-FRC façade panel. Results highlighted the applicability of the proposed methodology in facilitating the energy performance analysis of UHP-FRC panels

in different building contexts. This methodology can be used by designers as a decision support system to provide simple recommendations in the early stages of building envelope designs to obtain high-performance buildings.

These findings contribute to the body of knowledge by highlighting the applicability of proposed methodologies in investigating the energy performance of building façade panels in both assembly-scale and building context. It is expected that these methodologies provide building engineers with essential means to objectively appraise the energy performance of innovative façade systems in both assembly-scale and building context.

Table of Contents

Acknowledgements iv

Abstract v

Table of Contents ix

List of Tables xiii

List of Figures xv

Chapter 1 Introduction 18

1.1 Organization of Dissertation 21

Chapter 2 Background 22

2.1 Heat Transfer Analysis 22

2.2 Hygrothermal Assessment 23

2.3 Building Energy Performance Analysis 26

2.4 Uncertainty Analysis 26

2.5 Gaps in Knowledge 29

2.6 Research Objectives 29

Chapter 3 Heat Transfer and Hygrothermal Assessment of UHP-FRC Façade Panels 31

3.1 Methodology 31

3.1.1 Conventional Panels versus UHP-FRC Panels 32

3.1.2 Heat Transfer Analysis 35

3.1.3 Hygrothermal Analysis 37

3.2 Results and Discussion 38
3.2.1 Results of Thermal Bridging and Heat Transfer..... 38
3.2.2 Results of Moisture Transfer Analysis 41
Chapter 4 Transient Coupled Heat and Moisture Transfer Investigation 43
4.1 Methodology.....44
4.1.1 Panel Connections..... 47
4.1.2 Numerical Modeling of Heat, Air, and Moisture Transfer 48
4.1.3 Boundary and Initial Conditions..... 52
4.1.4 Numerical Simulations Tool..... 54
4.2 Illustration for UHP-FRC Facade Panel 54
4.2.1 Geometry and Material 54
4.2.2 Material Data 56
4.2.3 Simulation Parameters 59
4.3 Results and discussions.....61
4.3.1 Results of Heat Transfer 61
4.3.1 Results of Moisture Transfer 65
4.4 Conclusion 67
Chapter 5 Building Energy Performance Analysis of UHP-FRC Panels i 69
5.1 Methodology.....69
5.1.1 DOE Prototype Buildings 72
5.1.2 DOE Climate Zones and Representative Cities..... 75
5.1.3 Uncertainty Analysis..... 77

5.2 Results and Discussion 84
5.2.1 Results of Whole Building Energy Simulation..... 84
5.2.2 Impact of building operation schedules on the energy performance of UHP-FRC façade panels 89
5.2.3 T-test results..... 90
Chapter 6 Knowledge Discovery and Rule Extraction 93
6.1 Methodology 94
6.1.1 Building Energy Simulations..... 95
6.1.2 Building Context..... 98
6.1.3 DOE climate zones and representative cities..... 99
6.1.4 Scenarios under uncertainty..... 100
6.1.5 Building Energy Simulated Data 102
6.2 Knowledge Discovery.....103
6.2.1 Data Preprocessing..... 103
6.2.2 Clustering..... 104
6.2.3 Association Rule Mining 106
6.2 Results and Discussion 109
6.2.1 Descriptive Statistics..... 109
6.2.2 Results of Clustering Analysis..... 112
6.2.3 Results of Association Rule Mining 115
6.3 Validation.....118
Chapter 7 Conclusions and Future Work.....121

7.1 Conclusions.....121

7.2 Future Work.....123

References.....125

List of Tables

Table 1-1 Comparison of typical conventional concrete and UHP-FRC 19

Table 3-1 Thermo-physical properties of UHP-FRC and conventional panel assemblies 35

Table 3-2 Heat flows and heat fluxes in both cross-sections of UHP-FRC and conventional panel assemblies 41

Table 3-3 Moisture behavior behind the insulation layer and on the interior face of UHP-FRC and conventional panel assemblies, and maximum mold index during five years 42

Table 4-1 Thermo-physical properties of UHP-FRC and conventional panel assemblies 57

Table 4-2 Thermos-physical properties of constituent materials of UHP-FRC panel and steel connections 57

Table 5-1 Description of DOE prototype buildings 73

Table 5-2 Characteristics of DOE climate zones representativeness cities 76

Table 5-3 Uncertain parameters and their probability distributions 80

Table 5-4 Range of building operation parameters in good and poor practice 81

Table 5-5 The average annual building energy savings by replacing the conventional panel with UHP-FRC panel..... 85

Table 5-6 Descriptive statistics of annual energy use for mid-rise apartments with UHP-FRC and conventional façade panels..... 87

Table 5-7 The average annual medium office building energy savings by replacing the conventional panel with the UHP-FRC panel in good and poor operation practices 90

Table 5-8 T-test results 91

Table 6-1 Thermo-physical properties of UHP-FRC and conventional panels.... 97

Table 6-2 Spearman rank correlation between input variables..... 111

Table 6-3 Spearman rank correlation between input and output variables..... 111

Table 6-4 Attribute centroids and the number of instances within each cluster. 114

Table 6-5 Extracted association rules from Cluster 1, 2, and 4 116

Table 6-6 Description of selected buildings for validation..... 120

Table 6-7 Building energy savings 120

List of Figures

Figure 3-1 Simulation-based methodology for the energy performance analysis of UHP-FRC façade systems in assembly scale..... 32

Figure 3-2 Conventional and UHP-FRC façade panels configuration 34

Figure 3-3 Cross-sections of UHP-FRC and conventional panel assemblies..... 37

Figure 3-4 Heat flux magnitude in cross-section A and B of UHP-FRC and conventional panel assemblies..... 40

Figure 4-1 FEM-based methodology to numerically solve the transient heat and moisture transfer within UHP-FRC façade panel connections..... 46

Figure 4-2 Section view of non-share panel connections..... 47

Figure 4-3 UHP-FRC façade panel configuration 55

Figure 4-4 3D model of UHP-FRC panel connections..... 55

Figure 4-5 Thermos-physical properties of constituent materials of UHP-FRC panel and steel connections 58

Figure 4-6 Meshes generated for panel connections..... 59

Figure 4-7 Graphical representation of boundary conditions for panel connections 60

Figure 4-8 Ambient temperature and relative humidity for Miami International Airport in July 2019 for 3 months (90 days) evolution 61

Figure 4-9 Temperature distribution within panel connections after 3 months.... 62

Figure 4-10 Heat flux intensity within the cross-section of panel connection after 3 months..... 62

Figure 4-11 Heat flux directions within the cross-section of panel connections after 3 months..... 63

Figure 4-12 Maximum heat flux within the steel connections during 3 months .. 64

Figure 4-13 Minimum heat flux within the steel connections during 3 months... 64

Figure 4-14 Moisture flux in cross-section of panel connections after 3 months 65

Figure 4-15 Moisture flux directions within the cross-section of panel connections after 3 months 66

Figure 4-16 Relative humidity within panel connections after 3 months..... 66

Figure 5-1 Simulation-based methodology for the energy performance analysis of UHP-FRC façade systems in building context 71

Figure 5-2 3D model of DOE prototype buildings 74

Figure 5-3 Box plots of annual energy use for mid-rise apartments with UHP-FRC and conventional façade panels 88

Figure 6-1 Proposed framework for knowledge discovery and rule extraction.... 95

Figure 6-2 Conventional panel and UHP-FRC panel configuration..... 97

Figure 6-3 3D model of DOE prototype buildings 99

Figure 6-4 DOE climate zones and representative cities 100

Figure 6-5 Frequency distribution of input variables 110

Figure 6-6 Clustering validation with silhouette and Davies-Bouldin indexes .. 112

Figure 6-7 Representation of data points within four clusters in a two-dimensional feature space using two principal components 113

Figure 6-8 3D model of buildings used for validation..... 119

CHAPTER 1

INTRODUCTION

Residential and commercial buildings use approximately 40% of energy use in the United States (U.S. EIA, 2015). Majority of this amount of energy is used to heat and cool enclosed spaces in buildings (Park et al., 2015). Building façade systems control heat transmission between outdoor and indoor environments; therefore these systems can play a critical role in saving energy (Karasu, 2015).

In recent years, researchers have become increasingly interested in promoting energy efficiency and reducing energy consumption of buildings by finding innovative solutions. These solutions include the application of innovative materials such as ultra-high-performance fiber-reinforced concrete (UHP-FRC) (Bell et al., 2016), Fiber-reinforced Plastic (FRP) (Abdou et al., 1996), phase change materials (Sadineni et al., 2011; Iommi 2018), thermal resistance materials (Sadineni et al., 2011), and dynamic insulation materials (Park et al., 2015). They also include geometrical alterations of conventional façade systems (Hachem and Elsayed, 2016; Cheung et al., 2005), window shading (Cheung et al., 2005), and double reflective glazing (Chan et al., 2009). Although these studies provided valuable insight into the energy performance of innovative façade systems, they did not investigate the combined effect of different building types and climate conditions on the energy performance of these innovative façade systems.

Recent advances in concrete material innovation, such as UHP-FRC, offer the opportunity to reduce the energy loss through façade surfaces. UHP-FRC's compressive strength is six times higher than conventional concrete with a post-cracking tensile strain up to 0.6% without strength degradation (Aghdasi et al., 2016). Table 1 provides a comparison between typical conventional concrete and UHP-FRC (Kaka and Chao, 2018).

Table 1-1 Comparison of typical conventional concrete and UHP-FRC (all data from UT Arlington research except Rapid Chloride Penetration Test) (Kaka and Chao, 2018)

Properties of Concrete	**Conventional Concrete**	**UHP-FRC**
Ultimate Compressive Strength	< 8,000 psi (55 MPa)	18,000 to 30,000 psi (124 to 207 MPa)
Early (24-hour) compressive strength	< 3000 psi (21 MPa)	10,000 – 12,000 psi (69 to 83 MPa)
Flexural Strength	< 670 psi (4.6 MPa)	2,500 to 6,000 psi (17 to 41 MPa)
Shear strength	< 180 psi (1.2 MPa)	> 600 psi (4.1 MPa)
Direct Tension	< 450 psi (3 MPa)	up to 1,450 psi (10 MPa)
Rapid Chloride Penetration Test*	2000-4000 Coulombs passed	Negligible (< 100 Coulombs passed)
Ductility	Negligible	High ductility
Ultimate Compressive Strain, ε_{cu}	0.003	0.015 to 0.03
Confining	Negligible	High confining capability

* Ahlborn et al. 2011

The standard sandwich panels that are commonly used in façade systems of buildings range from 8 to 14 inches (20.32 to 35.56 cm) in thickness. UHP-FRC's ultra-high strength and ductility make it possible to consider altering building

strategies by creating a very thin and lightweight panel without conventional mild steel reinforcing bars (Bell et al., 2016). A UHP-FRC façade panel could have a thicker insulation layer (5 inches) compared with the conventional panel (2-inch insulation layer) (Bell et al., 2016). Although it is expected that buildings enhanced with UHP-FRC panels result in lower building energy consumption than buildings with the conventional panels, the energy performance assessment of innovative façade systems such as UHP-FRC panels could be misleading if the effect of building types and climate contexts on building energy consumption is not considered. Moreover, thermal bridging and hygrothermal analyses of UHP-FRC panels are needed to investigate the heat and moisture transfer within the panels in detail.

The ultimate goals of this research is to (1) analyze the heat and moisture transfer within the proposed UHP-FRC façade panel in a detailed assembly scale, (2) investigate the effect of panel connections in the hygrothermal performance of UHP-FRC façade panels, (3) investigate the combined effect of different building types and climate conditions on these panels' energy performance under uncertainty, and (4) knowledge discovery and pattern recognition for identifying and analyzing hidden underlying patterns in simulated data.

1.1 Organization of Dissertation

In order to achieve the objectives of this research, the remainder of this dissertation is organized as follows. Chapter 2 provides a comprehensive review of literature. This chapter reviews literature regarding heat transfer analysis, hygrothermal assessment, building energy simulation, and uncertainty analysis. Chapter 3 explains the methodology used for analyzing the thermal performance of UHP-FRC façade panels regarding thermal bridging and hygrothermal performance and provides the results. Chapter 4 present a hygrothermal assessment of panel connections. A 3D transient heat and moisture transfer approach is used to assess the effect of panel connections on the energy performance of UHP-FRC panels. In Chapter 5, a rigorous probabilistic methodology is developed and used for analyzing building energy performance of UHP-FRC façade panels compared with conventional façade panels. Moreover, the impact of building operations on the energy performance of the UHP-FRC panels is provided in this chapter. Chapter 6 presents a data mining approach that is developed to extract hidden information and underlying structures from the thermal behavior of a façade system in a limited set of scenarios. This framework provides easy to follow and simple rules on the energy performance of façade systems for different types of buildings in different climate zones. Finally, conclusions are presented in Chapter 7 and the contributions of this research to the state of knowledge and the state of practice are explicitly expressed.

CHAPTER 2

BACKGROUND

2.1 Heat Transfer Analysis

Building envelopes are the most important systems that affect buildings' energy performance. Since they are the major source of conductive heat losses in buildings. Therefore, a comprehensive assessment is needed to analyze the conductive heat transfer through the building envelope to identify the potential poor thermal behavior (Real et al., 2016). Changes in the geometry of constructive elements and properties of materials result in changes in thermal conductivity (Pessoa, 2011). Thermal bridges are parts of a panel system where their thermal resistance is usually lower than the adjacent areas (Real et al., 2016).

Thermal bridging is one of the concerns that is needed to be considered in the energy performance evaluation of new façade systems (Martin et al., 2011). Studies have shown that energy lost through thermal bridges in walls and roofs can be reached to 30% of heating energy uses in some buildings (Erhorn et al., 2010; Theodosiou & Papadopoulos, 2008). Therefore, addressing the thermal bridge issues in building envelope design is necessary (Ge & Zhang, 2013).

Several studies have been conducted to analyze the thermal bridging in façade systems. Hamza (2008) used numerical simulation ((IESVE Version 5.1) to analyze the impacts of double skin facade on cooling loads of office buildings in

hot arid areas like Cairo, the capital of Egypt. Theodosioua et al. (2017) used a detailed computational model within the ANSYS Workbench finite element analysis to evaluate the magnitude of thermal bridge effects in cladding systems and ventilated facades. They highlighted the effects of point thermal bridges in accelerating heat loss within such façade systems.

Although thermal bridging analysis can be used for thermal performance analysis of innovative facade systems in assembly scale, a detailed 3D heat transfer analysis is required to evaluate the thermal performance of innovative façade systems with complex configurations such as panel connections with the other building components like floors, roofs, and foundations. Results of a study conducted by ASHRAE show that the 3D thermal bridges such as corners, floor and wall connections, roof and wall junctions, and cladding attachment fasteners have higher contribution to the overall thermal transmittance of the assemblies (Roppel et al., 2012). This study has been carried out on 40 common building envelope details for mid- and high-rise construction.

2.2 Hygrothermal Assessment

Although having higher thermal resistance makes building envelope systems more energy-efficient, a new concern has to be considered regarding appropriate vapor diffusion control and moisture management (Mukhopadhyaya et

al., 2006). The risk of moisture condensation and mold growth in wall thermal layers is one of the major challenges in using interior thermal insulation systems (Pavlik & Cerny, 2009). Building envelopes protect the indoor environment from external forces arising from outdoor weather loads. Exterior walls expose to moisture and thermal loads (hygrothermal loads), while the interior side of walls experiencing different relative humidity and temperature conditions. As a result of the gradient arose from the differences in humidity and temperature between indoor and outdoor environments, water vapor or liquid moisture is transferred across the exterior which can coincide with dew point temperature and result in vapor condensation (Mukhopadhyaya et al., 2006). A prolonged duration of vapor present within the façade system can cause severe damage to the structure and environment.

Different manual analytical tools (such as dew point method, Glaser diagram, and Kieper diagram) have been used to analyze condensation within wall assemblies that are based on steady-state calculations of heat and moisture transfer (TenWolde, 2001). However, nowadays due to advancements in numerical algorithms and computer simulations, numerical simulations provide the opportunity to evaluate moisture behavior within façade panels not only in steady-state but also transient state.

A lot of research was done examining the hygrothermal behavior of exterior walls using numerical simulations. De Mets et al. (2017) conducted full-scale

laboratory tests and numerical simulations to analyze the hygrothermal performance of capillary active insulation systems. They used Delphin 5.8 for hygrothermal assessment of the system with different thicknesses of layers and boundary conditions. In another study, Vereecken et al. (2015) conducted a probabilistic analysis of energy savings and hygrothermal risks of a single leaf massive masonry wall outfitted with an interior insulation system for wall retrofitting purpose. They performed the analysis for different wall thicknesses and different exterior and interior climatic conditions using HAMFEM that solves the equations for energy and mass conservation based on a finite element method.

WUFI is a one or two-dimensional model for analyzing heat and moisture transfer developed by Fraunhofer Institute in Building Physics. This model provides a realistic calculation of the transient moisture transport within multilayer building components such as wall panels exposed to natural climate conditions (Künzel & Kiessl, 1996). This model is the most widely used hygrothermal assessment software (Delgado et al., 2010). Although WUFI and other numerical simulations provide great opportunity to evaluate hygrothermal assessment of innovative façade systems, the two-dimensional oversimplification does not support the analysis of thermal bridging through complex wall framing and connections (O'Grady et al., 2018; Garay et al., 2014; Doebber and Ellis, 2005; Kośny and Kossecka, 2002).

2.3 Building Energy Performance Analysis

Building energy performance analysis can be used for evaluating the performance of the building's façade, HVAC, lighting, water, and control systems (Crawley et al., 2000). In the last decades, a variety of building energy simulation programs have been developed to estimate future energy use of the buildings by simulating the complex interactions within buildings (Parent, 2002), such as BLAST, DOE-2.1E, ECOTECT, eQUEST, and EnergyPlus. Among all these building energy performance simulation tools, EnergyPlus has gained more attention in the U. S. due to its advantages. EnergyPlus has been widely used for estimating building energy performance in the practice and the research community because as a stand-alone whole building energy simulation tool, it models hourly energy use of buildings and gives the opportunity of manipulating construction, internal loads, schedules, and even weather by the users (Sailor, 2008).

2.4 Uncertainty Analysis

Uncertainty limits the confidence of building energy simulation results (Moon, 2005; Eisenhower et al., 2012), which may lead to a significant discrepancy between the simulation results and actual building energy consumptions. In recent studies, this issue with deterministic building simulations has been well addressed by the uncertainty analysis in recent studies.

The current literature on uncertainty analysis mostly emphasizes on identifying and quantification of uncertain parameters in the building energy performance analysis. Buildings are complex systems, characterized by multiple parameters, such as design geometry, material properties, occupancy levels, equipment schedules and operations, and climate and weather conditions (Coakley et al., 2014). Diverse sources of uncertainty originate from these parameters.

De Wit and Augenbroe (2002) classified these uncertain parameters into four categories: 1) specification uncertainty; 2) modeling uncertainty, which is mostly due to the simplifications and assumptions in the building models; 3) numerical uncertainty; and 4) scenario uncertainty.

A number of studies have been conducted to identify and quantify the impact of the above-mentioned uncertain parameters on building energy performance simulation outputs. In a comprehensive study, Eisenhower et al. (2012) conducted an uncertainty analysis to screen the most critical uncertain parameters in a building model. The authors considered more than 1000 uncertain parameters in the building energy performance process. They varied all nonzero parameters about 20% of their nominal values using uniform distribution and those with zero nominal value using exponential distribution. The authors performed a decomposition to quantify which subsystems have the most impact on the building energy uses. They found that cooling and heating setpoints are critical uncertain

parameters in terms of building heating and cooling loads. Moreover, occupancy and lighting schedules are dominating parameters in terms of zone internal loads.

Hopfe (2009) found that the heat conductivity of external wall components, equipment heat gains, and infiltration rate are the most critical uncertain parameters that are needed to be considered in the energy performance evaluation. In another research, Hopfe and Hensen (2011) considered physical properties and weather conditions as uncertain parameters and used them for supporting decision making in different climate conditions. In similar studies, occupancy level, indoor design condition, lighting loads, and weather-related uncertainties were recognized as critical parameters affecting the amount of building energy uses (Hopfe et al., 2007; Lam et al., 2008; Guerra-Santin and Itard, 2010; Sun et al., 2011; Bhandari et al., 2012; Li et al., 2015; Soto et al., 2015 and Berkeley et al., 2015; Berkeley et al., 2015; Menberg et al., 2016).

In a study done by de Wit and Augenbroe (2002), a general procedure is provided for uncertainty analysis. They originated the combination of uncertainty analysis with risk analysis in a decision-making context. The authors emphasized on quantifying model uncertainties using expert judgments where the uncertainty cannot be estimated using statistical methods. They found that the combination of expert judgment and statistical methods shows promising outputs in quantifying the impact of uncertainties in building energy models.

2.5 Gaps in Knowledge

Although the existing studies have added valuable insight into energy performance analysis of innovative building façade panels, yet there are significant gaps in knowledge related to energy performance analysis of UHP-FRC façade panels:

- There is no empirical or simulation-based on heat and moisture behaviors within the UHP-FRC panels in the assembly scale;
- The oversimplification in heat and moisture transfer analysis can lead to either overestimation or underestimation in building energy consumptions; and
- There is no empirical or simulation-based data to present the energy performance of UHP-FRC panels in assembly scale and building context;
- Results of building energy performance simulations do not provide a practical guideline to support decision-making;

2.6 Research Objectives

The primary objectives of this research are organized into four main sets as follows:

1. Investigate the heat and moisture transfer within the UHP-FRC façade panel assemblies in different boundary conditions;
2. Investigate transient three-dimensional heat and moisture transfer within the UHP-FRC façade panel assemblies in different panel connections;
3. Investigate the combined effect of different building types and climate conditions on these panels' energy performance under uncertainty;
4. Discover underlying structure, pattern, and interactions among energy performance, building design parameters, external simulation parameters using data mining techniques.

These objectives are addressed in the next following chapters, respectively.

CHAPTER 3

HEAT TRANSFER AND HYGROTHERMAL ASSESSMENT OF UHP-FRC FAÇADE PANELS

The heat and moisture transfer within the innovative UHP-FRC panels should be rigorously evaluated using proper methods to assure that the innovative panel does not exacerbate heat loss through thermal bridges, and there is no risk of mold growth behind the insulation layer of the panels. The objective of this chapter is to investigate the heat and moisture transfer within the UHP-FRC façade panel assemblies by conducting transient hygrothermal performance analysis using a numerical simulation for different boundary conditions.

3.1 Methodology

Figure 3-1 presents the process to evaluate the energy performance of the UHP-FRC façade systems in comparison with the performance of the conventional façade systems in the assembly scale. Thermal bridging analysis and hygrothermal assessment were conducted in detail for both panel assemblies. The thermal bridging analysis was conducted for six different boundary conditions. The hygrothermal assessment of panel assemblies was also conducted to compare the moisture behavior within the panels in fifteen locations across the U.S.

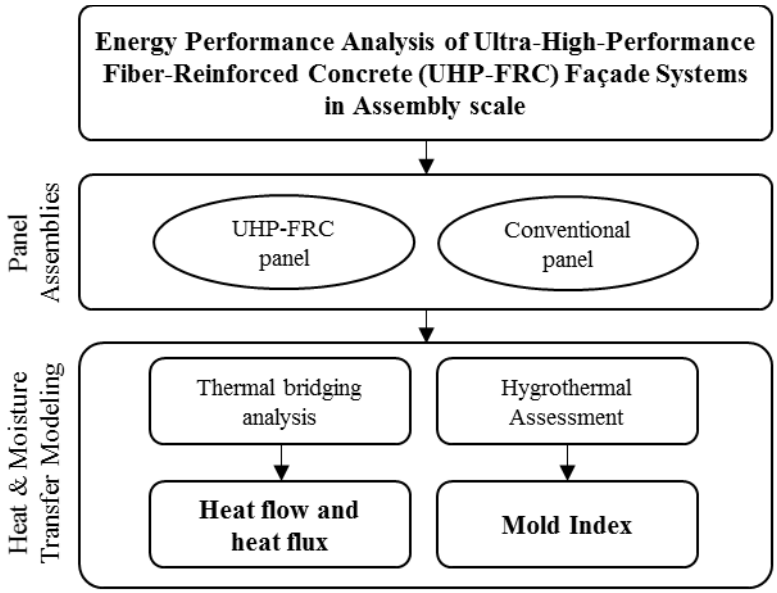

Figure 3-1 Simulation-based methodology for the energy performance analysis of UHP-FRC façade systems in assembly scale

3.1.1 Conventional Panels versus UHP-FRC Panels

The 8-inch thick standard conventional panel, which is commonly used in the U.S. construction industry (Losch et al., 2011), with a weight of 676 lbs. is used as a baseline in this research. It consists of three layers: a 3 inch (7.62 cm) facing Wythe, 2 inches (5.08 cm) Expanded Polystyrene (EPS) rigid insulation, and 3 inches (7.62 cm) structural backing wythe. A standard 7-sack Portland cement mix is used to produce compression strength of 5,000 psi for the facing mix and 7,000 psi compression strength for the backing mix. The wythes are structurally reinforced with a 6 inch by 6 inch (15.24 by 15.24 cm) wire mesh, which is attached to a NO.4 - 1/2 inch (1.27 cm) - rebar around the panel parameter. Two wythes are

connected with standard connection ties (ThermoMass T Series Fiberglass) together connecting through the insulation layer while limiting the amount of thermal bridging (Bell et al., 2016).

The innovative UHP-FRC pre-cast sandwich panel is comparable to the industry standard panel. This panel consists of a 1-1/2 inch (3.81 cm) UHP-FRC facing wythe, a 5 inch (12.7 cm) Extruded Polystyrene (XPS) rigid insulation and a 1-1/2 inch (3.81 cm) UHP-FRC backing wythe with the weight of 338 lbs. The structural layers are connected with standard connection ties (ThermoMass CC130 Fiberglass connector). All reinforcing bars are eliminated, which helps to provide more space for the insulation layer. Removing reinforcing bars also reduce fabrication work and time. This panel provides three times higher cracking resistance compared to the conventional façade panel even without reinforcing bars (Bell et al., 2016). Figure 3-2 shows the configurations of both façade panels.

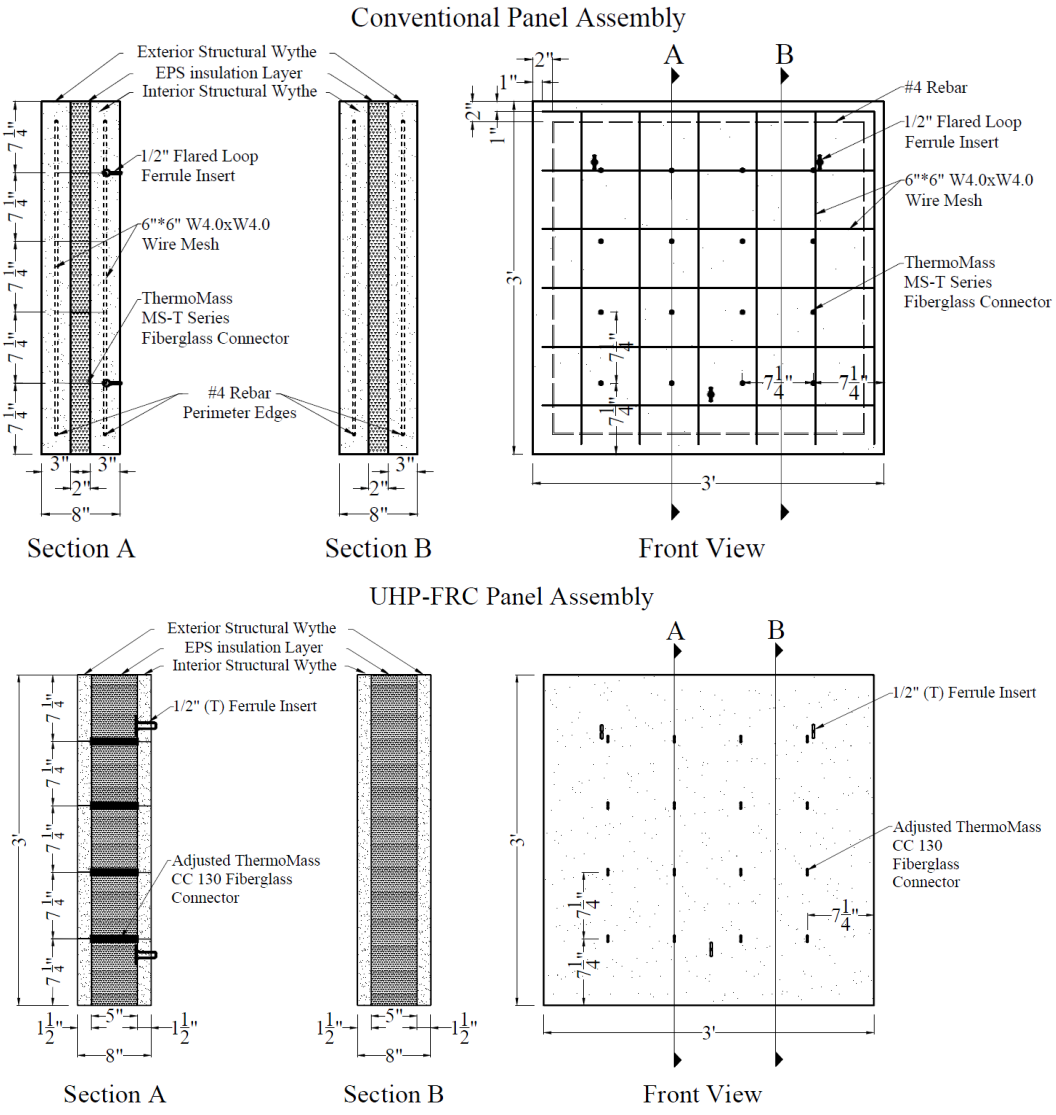

Figure 3-2 Conventional and UHP-FRC façade panels configuration (Section A, B, and front view)

Numerical analyses of heat and moisture transfer through UHP-FRC and conventional panel assemblies are carried out to investigate the significance of thermal bridging and the risk of mold growth within the panels. The thermal and

moisture transfer analyses are used to find the thermal linkage between the exterior and interior sides of the panels. Table 3-1 shows the thermal and hygrothermal properties of panel layers in both UHP-FRC and conventional panel assemblies used in the numerical simulations.

Table 3-1 Thermo-physical properties of UHP-FRC and conventional panel assemblies

Items	Parameters	Unit	Conventional Panel	UHP-RFC Panel
Concrete layer	Thickness (D)	cm	7.62 (3 in)	3.81 (1.5 in)
	Density (ρ)	kg/m3	2322	2403
	Porosity (P)	m3/m3	0.7912	0.7912
	Specific heat capacity (Cp)	J/kg-K	832	1010
	Thermal conductivity (λ)	W/m-K	2.31	1.77
	Vapor diffusion resistance (μ)	-	18.58	18.58
	Initial moisture content (MC)	kg/m3	19.22	20
Insulation layer	Thickness (D)	cm	5.08 (2 in)	12.7 (5 in)
	Density (ρ)	kg/m3	28	20
	Porosity (P)	m3/m3	0.99	0.99
	Specific heat capacity (Cp)	J/kg-K	645	645
	Thermal conductivity (λ)	W/m-K	0.005769	0.005769
	Vapor diffusion resistance (μ)	-	73.02	170.55
	Initial moisture content (MC)	kg/m3	0.06	0.13

3.1.2 Heat Transfer Analysis

Building façade systems, which are separating indoor and outdoor environments, are the major source of conduction heat losses in buildings. Heat losses happen through the elements of building façade panels as well as thermal bridges. Thermal bridges are parts of a panel system where their thermal resistance

is usually lower than the adjacent areas (Real et al., 2016). Hence, they originate additional heat exchange between the exterior and interior environments. Therefore, thermal bridging is one of the concerns that is needed to be considered in the energy performance evaluation of new façade systems.

The thermal bridging analysis of both UHP-FRC and conventional panel assemblies is performed to compare the energy performance of both panels in the assembly scale. A finite element method is used to model the heat transfer behavior within the UHP-FRC and conventional panel assemblies. THERM 7.4 (Mitchell et al., 2003; Ge et al., 2013) employs Finite Quadtree meshing algorithm and model heat transfer. The detailed configurations (Figure 3) of the panels including rebars in conventional panels and fiberglass connectors in UHP-FRC panels are used in the thermal bridging analysis considering five boundary conditions (different exterior and interior temperatures). Figure 3-3 illustrates the model of UHP-FRC and conventional façade panels in section A and Section B.

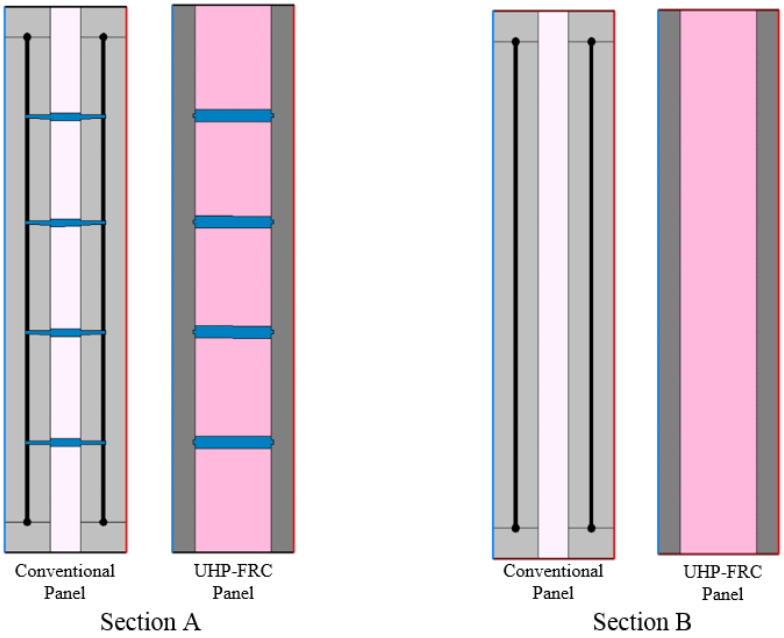

Figure 3-3 Cross-sections of UHP-FRC and conventional panel assemblies used in the simulations

3.1.3 Hygrothermal Analysis

The risk of moisture condensation and mold growth in wall thermal layers is one of the major challenges in using interior thermal insulation systems (Pavlík & Černý, 2009). Condensation mostly happens on the cold side of the insulation layer in exterior walls due to water content increase (Finken et al., 2016). This condensation typically leads to mold problems. Since a thicker insulation layer is used in the UHP-FRC panel assembly, the hygrothermal analysis of this panel assembly is conducted. Heat and moisture transient method is used to conduct the hygrothermal analysis. WUFI Pro 6.2 (Zirkelbach et al., 2007) is used to model the coupled moisture and heat transfer within both UHP-FRC and conventional panel

assemblies. WUFI also provides the mold index (MI), which shows the risk of mold growth in a six-point scale, where the mold index of 6 means the highest level of mold growth risk, 1 means the tolerable level of risk, and 0 mean no risk of mold growth. The WUFI mold index criterion is based on the ASHRAE standard 160.

The hygrothermal analysis of UHP-FRC and conventional panel assemblies are carried out using WUFI in fifteen locations within the U.S. It is assumed that the panel assemblies are vertically installed. The orientation of panels is set to the directions that are most exposed to driving rain for each location (based on WUFI's historical weather data). The indoor temperature and moisture loads are set according to ASHRAE 160 standard (heating setpoint: 21.1 °C, cooling setpoint: 23.9 °C, and relative humidity: 80% RH). The initial moisture and temperature for all the components are selected as constant (20 °C; 80% RH). The simulation duration is set to 10 years from January 2011 to December 2019.

3.2 Results and Discussion

3.2.1 Results of Thermal Bridging and Heat Transfer through Panel Assemblies

Figure 3-4 shows the results of thermal bridging analysis regarding the heat transfer within Section A and B of UHP-FRC and conventional panel assemblies for five different boundary conditions (five different indoor and outdoor temperature differences). The thermal bridging result for Section A of the

conventional panel shows that the thermal bridging in the conventional panel happens not only at the location of the connectors but also at the location of the structural rebars. The results of thermal bridging clearly show that combination of connectors and rebars is accelerating the thermal bridging in the conventional panel. In contrast, the heat transfer results for the UHP-FRC panel for all the boundary conditions show that the connectors are the only reason for thermal bridging. Moreover, the heat flux results for Section A of both panels show that as the temperature difference increases between indoor and outdoor environments, heat flux intensity increases in the conventional panel but not the UHP-FRC panel.

The results of thermal bridging for Section B of the UHP-FRC assembly show that the amount of thermal bridging of the UHP-FRC panel is negligible and changes in temperature differences do not affect the heat flux intensity. On the other hand, although the amount of thermal bridging in Section B of the conventional panel is low since there is no connector in this section, the perimetrical structural rebars placed on the edges of the panel increases the heat flux mostly in the edges of the conventional panel. Table 3-2 shows the results of the thermal bridging analysis for both assemblies in detail. The heat flow and heat flux in both sections of both panel assemblies show that the UHP-FRC panel assembly performs better in all boundary conditions in terms of thermal resistance. The R-value for UHP-FRC panel assembly is 0.87 for Section A and 0.27 m^2-K/W for Section B. On the

other hand, the conventional panel's R-values are 0.12 and 0.35 m^2-K/W for Section A and B, respectively.

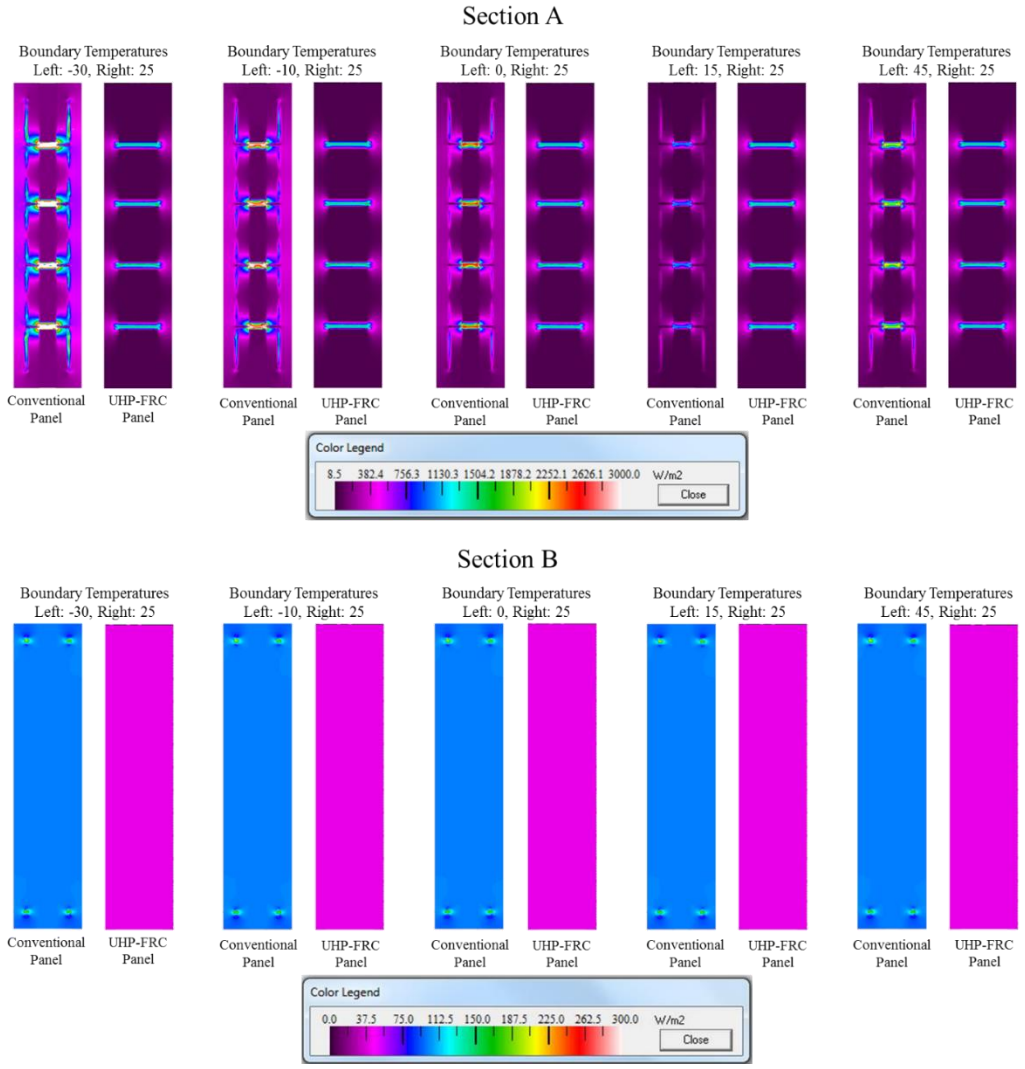

Figure 3-4 Heat flux magnitude in cross-section A and B of UHP-FRC and conventional panel assemblies

Table 3-2 Heat flows and heat fluxes in both cross-sections of UHP-FRC and conventional panel assemblies

Section	Boundary temperature (Out-In)	Delta (°C)	Parameter	Conventional panel	UHP-RFC panel
Section A	-30 °C - 25 °C	55	Heat flow (W)	17.0	7.3
			Heat flux (W/m^2)	472.2	203.1
	-10 °C - 25 °C	35	Heat flow (W)	10.8	4.7
			Heat flux (W/m^2)	300.5	129.2
	0 °C - 25 °C	25	Heat flow (W)	7.7	3.3
			Heat flux (W/m^2)	214.6	92.3
	15 °C - 25 °C	10	Heat flow (W)	3.1	1.3
			Heat flux (W/m^2)	85.9	36.9
	45 °C - 25 °C	-20	Heat flow (W)	6.2	2.7
			Heat flux (W/m^2)	171.7	73.8
Section B	-30 °C - 25 °C	55	Heat flow (W)	5.7	2.3
			Heat flux (W/m2)	157.5	63.0
	-10 °C - 25 °C	35	Heat flow (W)	3.6	1.4
			Heat flux (W/m2)	100.2	40.1
	0 °C - 25 °C	25	Heat flow (W)	2.6	1.0
			Heat flux (W/m2)	71.6	28.6
	35 °C - 25 °C	-10	Heat flow (W)	1.0	0.4
			Heat flux (W/m2)	28.6	11.5
	45 °C - 25 °C	-20	Heat flow (W)	2.1	0.9
			Heat flux (W/m2)	57.3	22.9

3.2.2 Results of Moisture Transfer Analysis within Panel Assemblies

Table 8 presents the results of the hygrothermal analysis of both UHP-FRC and conventional panel assemblies in terms of relative humidity and mold index for the ten years. The results show that the relative humidity behind the insulation layer in both UHP-FRC and conventional panels are less than 80%. However, the relative humidity on the interior side of the UHP-FRC panel assembly is slightly lower than the relative humidity on the interior side of the conventional panel assembly in all the locations.

The relative humidity percentages on the interior side of the panel assemblies show that the UHP-FRC panel performs better than conventional panels even in Miami, where the relative humidity of the conventional panel on its interior side passes 80% threshold. Moreover, the results for mold index show that the risk of mold growth is 0 (6 highest and 0 no risk) behind the insulation layers of the UHP-FRC panel assembly in all locations. Similar mold indexes have been achieved for the conventional panel assembly for all locations.

Table 3-3 Moisture behavior behind the insulation layer and on the interior face of UHP-FRC and conventional panel assemblies, and maximum mold index during five years

Relative humidity / City	Orientation	Conventional panel				UHP-RFC panel			
		Interior surface		Behind insulation layer		Interior surface		Behind insulation layer	
		RH (%)	Mold index	RH > 80%	Mold index	RH (%)	Mold index	RH > 80%	Mold index
Fairbanks	SW	26-73	0	No	0	22-73	0	No	0
Duluth	E	27-75	0	No	0	23-73	0	No	0
Helena	N	28-74	0	No	0	25-72	0	No	0
Burlington	SW	27-77	0	No	0	25-73	0	No	0
Chicago	NE	28-76	0	No	0	25-74	0	No	0
Boise	W	28-73	0	No	0	26-70	0	No	0
Albuquerque	E	22-73	0	No	0	26-72	0	No	0
San Francisco	SW	43-76	0	No	0	40-76	0	No	0
Salem McNary	S	36-76	0	No	0	34-74	0	No	0
Baltimore	NE	27-76	0	No	0	25-73	0	No	0
Memphis	S	29-75	0	No	0	26-73	0	No	0
El Paso	W	20-74	0	No	0	30-71	0	No	0
Houston	NE	34-77	0	No	0	32-74	0	No	0
Phoenix	E	17-70	0	No	0	26-70	0	No	0
Miami	SE	46-84	0	No	0	43-77	0	No	0

CHAPTER 4

TRANSIENT COUPLED HEAT AND MOISTURE TRANSFER INVESTIGATION OF FAÇADE PANEL CONNECTIONS

Over the last decades, a significant effort has been devoted to reducing building energy consumptions by improving the energy efficiency of building facade systems. Recent advances in material innovation, such as ultra-high-performance fiber-reinforced-concrete (UHP-FRC), offer the opportunity to reduce energy loss through façade systems. While these advancements provide a potential for the development of energy-efficient facade panels, investigating the effect of façade connections in the thermal performance of façade systems is overlooked. The oversimplification in complex wall connections and ignoring the hygroscopic behavior of materials can lead to either overestimation or underestimation in the energy performance analysis of building façade systems. The main objective of this chapter is to investigate the effect of panel connections in the hygrothermal performance of façade panels. A transient, coupled heat and moisture transfer analysis has been conducted in order to investigate the effect of panel connections in the hygrothermal behavior of facade panels. Governing partial differential equations for coupled heat and moisture transfer were formulated. Four panel connections proposed by Precast/Prestressed Concrete Institute (PCI) were modeled for the UHP-FRC facade panel as an illustration, and a finite element

method (FEM) was used to solve the numerical models. The results of heat transfer analysis showed that steel connections could significantly reduce the thermal resistivity of façade panels by converging heat fluxes and acting as thermal bridges within façade panels. The results also showed that the maximum heat flux in the steel connector of the panel to foundation connection had ten times higher compared to the other connections. In addition, the results of moisture transfer showed that air gaps between the panels had higher moisture flux compared to the other layers in the connections. Therefore, new connection designs and materials seem to be essential for innovative façade systems to effectively exploit the potential opportunities provided by innovative façade systems. The results show the significant importance of connections in the energy performance analysis of façade systems. These findings contribute to the body of knowledge by highlighting the applicability of the proposed methodology to investigate the heat and moisture transfer in different building façade panel connections. It is expected that the results will be used by facade designers for further thermal investigation in façade connections.

4.1 Methodology

A numerical transient heat and moisture transfer is proposed to investigate the effect of panel connections in the hygrothermal performance of façade panel

systems. Figure 4-1 illustrates a step by step procedure of the proposed framework. First, the required information, such as the geometry of panel connections, material properties, initial conditions, and ambient weather information, is collected. Then, 3D model of panel connections is developed. Initial and boundary conditions are set for models. The governing partial differential equations are defined for heat and moisture transfer, then solved using a finite element method (FEM). Temperature, heat, and moisture flux within domains are calculated and extracted from the solutions, and further investigated to assess the risk of mold growth. These steps are further elaborated in the following sections.

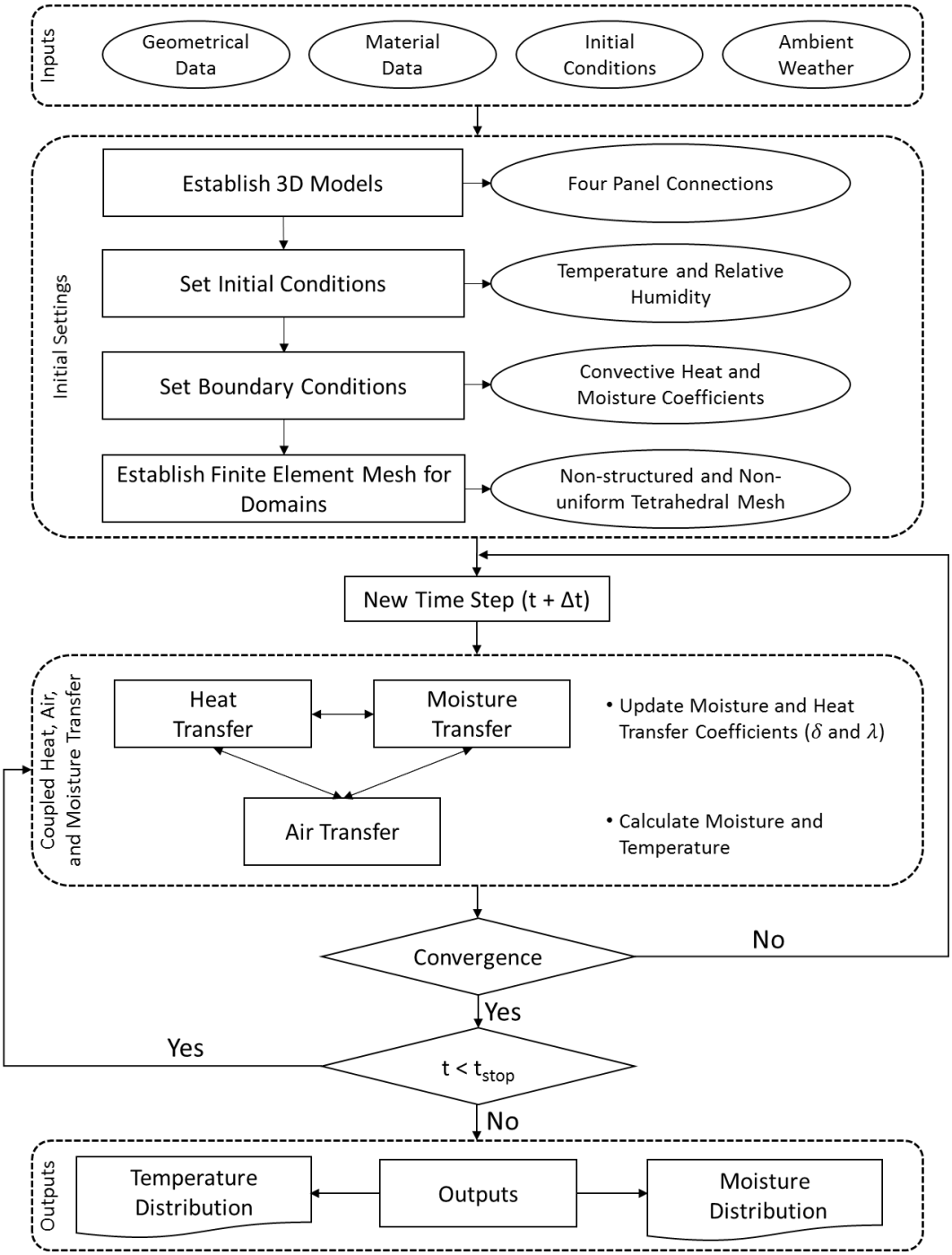

Figure 4-1 FEM-based methodology to numerically solve the transient heat and moisture transfer within UHP-FRC façade panel connections

4.1.1 Panel Connections

Two panel to panel corner connections, one panel to intermediate floor connection, and one panel to foundation connection proposed by Precast Concrete Institute (PCI) are modeled in this study to analyze the effect of connections on the hygrothermal performance of façade panels. Figure 4-2 illustrates the section view of four panel connection.

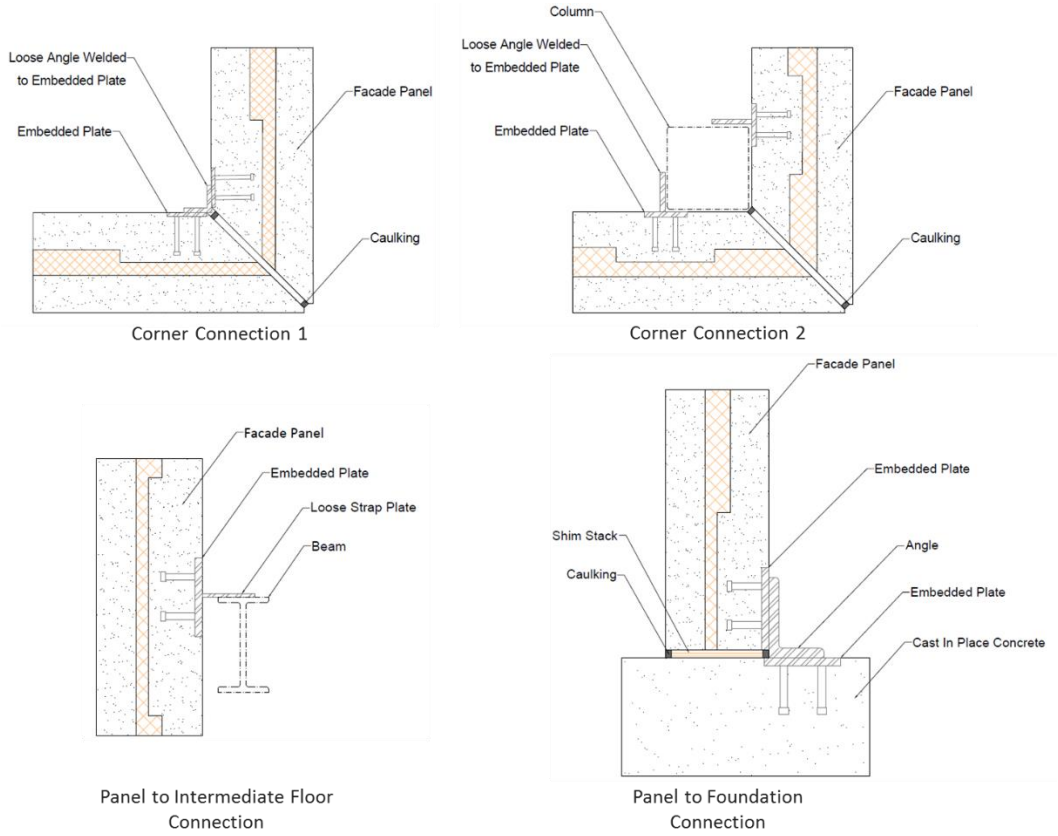

Figure 4-2 Section view of non-share panel connections

4.1.2 Numerical Modeling of Heat, Air, and Moisture Transfer

Coupled transient heat, air, and moisture transfer (HAM) in a porous material involves complex physical phenomena. This complexity depends on the mutual effect of heat, air, and mass transfer on each other (Maliki et al., 2017). Liquid and vapor are two different phases of moisture that can transfer within building materials (Balocco and Petrone, 2018). Vapor can transfer by diffusion or convection. Vapor diffusivity occurs in a porous media due to the pressure gradient, while convective vapor flow is advected by airflow (Steeman et al., 2009). On the other hand, moisture content gradient can be used as a driving potential for liquid flow, and moisture diffusivity as the driving potential for moisture transfer conductivity (Maliki et al., 2017). Governing equations of coupled mass transfer in building porous materials can be formulated based on the principle of the preservation of the combined heat and humidity of a representative elementary volume.

4.1.2.1 Air Transfer

In this study, the air transfer is included implicitly in the mass and heat conservation equations. By assuming the airflow as constant and moisture content independent, the dry-air mass balance can be expressed by Eq. 4-1:

$$\partial \rho_a / \partial t = v . \rho_a \qquad \text{Equation 4-1}$$

Where ρ_a is the dry air density, and v is the airflow velocity.

4.1.2.2 Moisture Transfer

Moisture transfer through a porous media can occur in both vapor and liquid phases (Eq. 4-2):

$$g = g_l + g_v \quad \text{Equation 4-2}$$

g_l is described by Darcy's law as liquid flux:

$$g_l = -K_l \nabla P_C \quad \text{Equation 4-3}$$

Where K_l (s) is liquid water permeability, and P_C is the capillary pressure. On the other hand, moisture can be transferred by diffusion and convection when it is in the vapor phase. Therefore, vapor flow in a porous media can be described as (Eq. 4- 4):

$$g_v = -\delta_P \nabla P_v + \rho_v v \quad \text{Equation 4-4}$$

Where δ_P is the vapor permeability, p_v is the partial water vapor pressure, v is the air velocity, and ρ_v is the water vapor density. The mass balance can be expressed by the following equation:

$$\frac{\partial w}{\partial t} + \nabla . g = 0 \quad \text{Equation 4-5}$$

Where w (kg/m^3) is moisture content, and t is the time. The moisture content can be expressed in terms of capillary pressure derivative the same as follows:

$$\frac{\partial w}{\partial t} = (\frac{\partial w}{\partial P_c}).(\frac{\partial P_c}{\partial t}) \quad \text{Equation 4-6}$$

The relation of potential flow initiated by relative humidity and the capillary pressure is expressed in Eq. 4-7. This equation is defined by Kelvin's law:

$$P_c = \rho_l R_v T ln\varphi \quad \text{Equation 4-7}$$

Where ρ_l is the water density, and R_V is the gas constant for water vapor. Now, by substitution of all the equations above, governing moisture content is expressed by Eq.4-8:

$$\frac{\partial w}{\partial \varphi}\frac{\partial \varphi}{\partial t} = \nabla.(K_l \nabla P_C) + \nabla.\delta_P(\frac{P_v}{P_v}\nabla P_C + (\varphi\frac{\partial P_{sat}}{\partial T} - \frac{P_v ln\varphi}{T})\nabla T) - v.\nabla\rho_v \quad \text{Equation 4-8}$$

4.1.2.3 Heat Transfer

In a transient state, heat can transfer by conduction and convection if it is assumed that there is no heat source within the medium. Therefore, the general form of heat transfer can be expressed by Eq. 4-9:

$$q = q_{conduction} + g_{convection} \quad \text{Equation 4-9}$$

Conductive heat transfer within the media can be expressed by Eq. 4-10:

$$q_{conduction} = -\lambda . \nabla T \quad \text{Equation 4-10}$$

Where λ is the thermal conductivity, and T is the temperature. Convective heat transfer is also expressed by Eq. 4-11:

$$q_{convection} = v\rho_a C_{P,a} \nabla T + g_v L_v \quad \text{Equation 4-11}$$

Where L_v is latent heat from vaporization, ρ_a is dry air density, and $C_{P,a}$ is the heat capacity of dry air. Now, the energy balance equation is expressed by Eq. 4-12:

$$-\nabla . q = (C_{P,m}\rho_m + C_{P,l} w)(\frac{\partial T}{\partial t}) \quad \text{Equation 4-12}$$

Where $C_{P,m}$ and ρ_m are the dry specific heat and dry density of the material, respectively. $C_{P,l}$ is the specific heat of liquid water. The effective volumetric capacity at constant pressure, which is defined to account for both solid and moisture properties, can be expressed by Eq. 4-13:

$$(\rho C_p)_{eff} = \rho_s C_{p,s} + w C_{p,w} \quad \text{Equation 4-13}$$

Where ρ_s is the dry solid density, $C_{p,s}$ is the dry solid specific heat capacity, *w* is the water content from moisture storage function for the selected material, and $C_{p,w}$ is the water heat capacity in constant pressure. Similarly, the effective thermal conductivity is defined to account for both solid and moisture properties (Eq. 4-14):

$$k_{eff} = k_s(1 + \frac{bw}{\rho_s}) \quad \text{Equation 4-14}$$

Where k_s is the dry solid thermal conductivity, and b is the thermal conductivity supplement due to water content. Now, by substituting the effective volumetric capacity and thermal conductivity in the energy balance equation, the coupled thermal analysis can be solved by Eq. 4-15:

$$\left(\rho C_p\right)_{eff}\left(\frac{\partial T}{\partial t}\right) = \nabla.(k_{eff}.\nabla T) + L_v\nabla.(\delta_p\nabla p_V) - v.(L_v\nabla p_V + \rho_a C_{P,a}\nabla T) \qquad \text{Equation 4-15}$$

4.1.3 Boundary and Initial Conditions

Boundary and initial conditions should be selected wisely to achieve high accuracy in hygrothermal simulations. Mass diffusion occurs within two sides of a multilayer façade due to temperature and moisture gradient that affects the mass balance (Chang & Weng, 2000). Therefore, the boundary condition for heat transfer at both sides of the multilayer façade panel can be described as Eq. 4-16 in terms of convection heat flux.

$$q = h(T_{air} - T_{surface}) \qquad \text{Equation 4-16}$$

Where q is the heat flux density (W/m^2) in the external and internal panel surfaces, T_{air} is the ambient air temperature (K), $T_{surface}$ is the surface temperature of the panel material (K), and h is the total heat transfer coefficient (W/m^{2}K). Total heat transfer coefficient (h) consists of two parts including convective and radiation-

related heat transfer coefficients. In this study, h is chosen 25 and 5 (W/m^{2}K) for the exterior and interior surfaces of the panel, respectively.

Similarly, the boundary condition for moisture transfer at both sides of the multilayer façade panel can be described as Eq. 4-17 in terms of convection moisture flux and pressure difference.

$$g = \beta(p_{air} - p_{surface}) \quad \text{Equation 4-17}$$

Where, g is the vapor diffusion density (kg/m^2.s) in the external and internal panel surfaces, β is the water vapor transfer coefficient (kg/m^2.s.Pa), p_{air} is the partial pressure of water vapor in the ambient air (Pa), and $T_{surface}$ is the partial pressure of the building material (Pa). Since there are similarity relations between water vapor transfer and heat transfer, so that β for exterior and interior surfaces of the panel can be obtained using Eq.18:

$$\beta = 7.0E-09 \, . \, h_c \quad \text{Equation 4-18}$$

Where h_c is the convective component of the heat transfer coefficient. Conversely, temperature and moisture content are continuous at the interfaces between the internal layers. Therefore, boundary conditions can be given in the interface of two building layers (l_x, l_{x+1}) as:

$$T(l_x, t) = T(l_{x+1}, t), \; x = 1,2, \dots, n \quad \text{Equation 4-19}$$
$$\varphi(l_x, t) = \varphi(l_{x+1}, t) \qquad x = 1,2, \dots, n \quad \text{Equation 4-20}$$

Initial conditions for all the panel materials are set to 50% for relative humidity, 19 °C (292.15 K) for temperature, and 10^3 Pa (1 atm) for water vapor pressure.

4.1.4 Numerical Simulations Tool

Governing equations for the coupled heat, air, and moisture transfer within the façade panels and their boundary conditions are numerically solved using a finite element method (FEM) based approach. COMSOL Multiphysics v5.2 (2013) time-dependent solver is used to solve the transient coupled partial differential equations (PDEs).

4.2 Illustration for UHP-FRC Facade Panel

4.2.1 Geometry and Material

Figure 4-3 illustrates the configuration of the UHP-FRC panel configuration (Section A, B, and front view). The UHP-FRC pre-cast sandwich panel is comparable to the industry standard panel. This panel consists of a 1–1/2 inch (3.81 cm) UHP-FRC facing wythe, a 5 inch (12.7 cm) Extruded Polystyrene (XPS) rigid insulation, and a 1–1/2 inch (3.81 cm) UHP-FRC backing wythe. The structural layers are connected with standard connection ties (ThermoMass CC130

Fiberglass connector). Figure 4-4 illustrates the 3D model of UHP-FRC panel connections used in this study. These connections are designed based on the recommendation of the Precast/Prestressed Concrete Institute (PCI) Committee on Precast Sandwich Wall Panels (Losch et al., 2011).

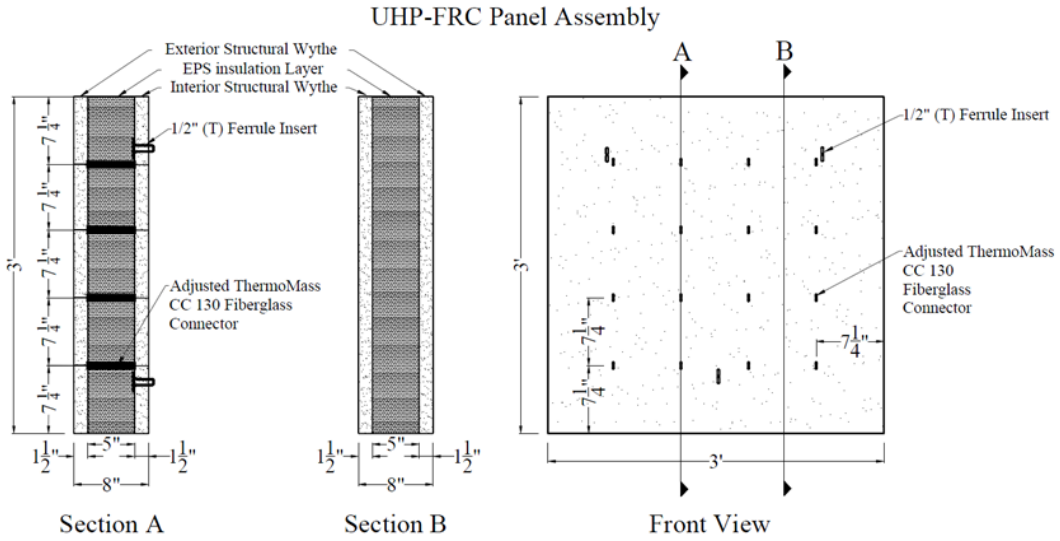

Figure 4-3 UHP-FRC façade panel configuration (Section A, B, and front view)

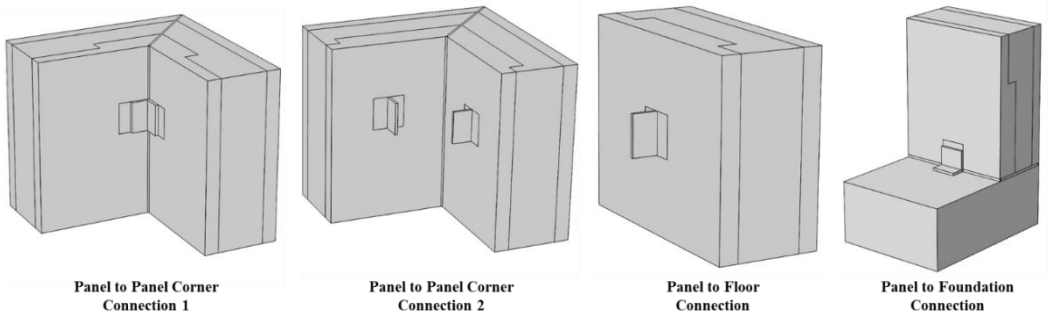

Figure 4-4 3D model of UHP-FRC panel connections

4.2.2 Material Data

Table 4-1 shows the thermal and hygrothermal properties of UHP-FRC panel materials used in the numerical simulations. In addition, moisture storage functions (sorption isotherm) of UHP-FRC and the insulation layer (XPS), the temperature-dependent density of steel, the temperature-dependent specific heat capacity of steel and Fiberglass connectors, and relative humidity dependent heat conductivity of UHP-FRC are obtained from WUFI (2007) material library to accommodate the dependencies in the simulations. Table 4-2 shows these dependencies in thermo-physical properties of the UHP-FRC constituent materials and steel connections. Figure 4-5 illustrates the correlation curves between the thermos-physical property of materials respect to relative humidity and temperature.

Table 4-1 Thermo-physical properties of UHP-FRC and conventional panel assemblies

Items	Parameters	Unit	UHP-RFC Panel
Concrete layer	Thickness (D)	cm	3.81 (1.5 in)
	Density (ρ)	kg/m3	2403
	Porosity (P)	m3/m3	0.7912
	Specific heat capacity (Cp)	J/kg-K	1010
	Thermal conductivity (λ)	W/m-K	1.77
	Vapor diffusion resistance (μ)	-	18.58
	Initial moisture content (MC)	kg/m3	20
Insulation layer	Thickness (D)	cm	12.7 (5 in)
	Density (ρ)	kg/m3	20
	Porosity (P)	m3/m3	0.99
	Specific heat capacity (Cp)	J/kg-K	645
	Thermal conductivity (λ)	W/m-K	0.005769
	Vapor diffusion resistance (μ)	-	170.55
	Initial moisture content (MC)	kg/m3	0.13

Table 4-2 Thermos-physical properties of constituent materials of UHP-FRC panel and steel connections

Thermo-physical Properties	UHP-FRC	Insulation Layer (XPS)	Connections (Steel)	Panel Layers Connectors (Fiberglass)
ρ [kg/m^3]	2403	20	$\rho(T)$	91.4
$\boldsymbol{c_p}$ [J/kg.K]	1010	645	$c_p(T)$	$c_p(T)$
$\boldsymbol{\lambda}$ [W/m.K]	$\lambda(\varphi)$	0.025	50.2	$\lambda(T)$
w [kg/m^3]	$w(\varphi)$	$w(\varphi)$	0	0

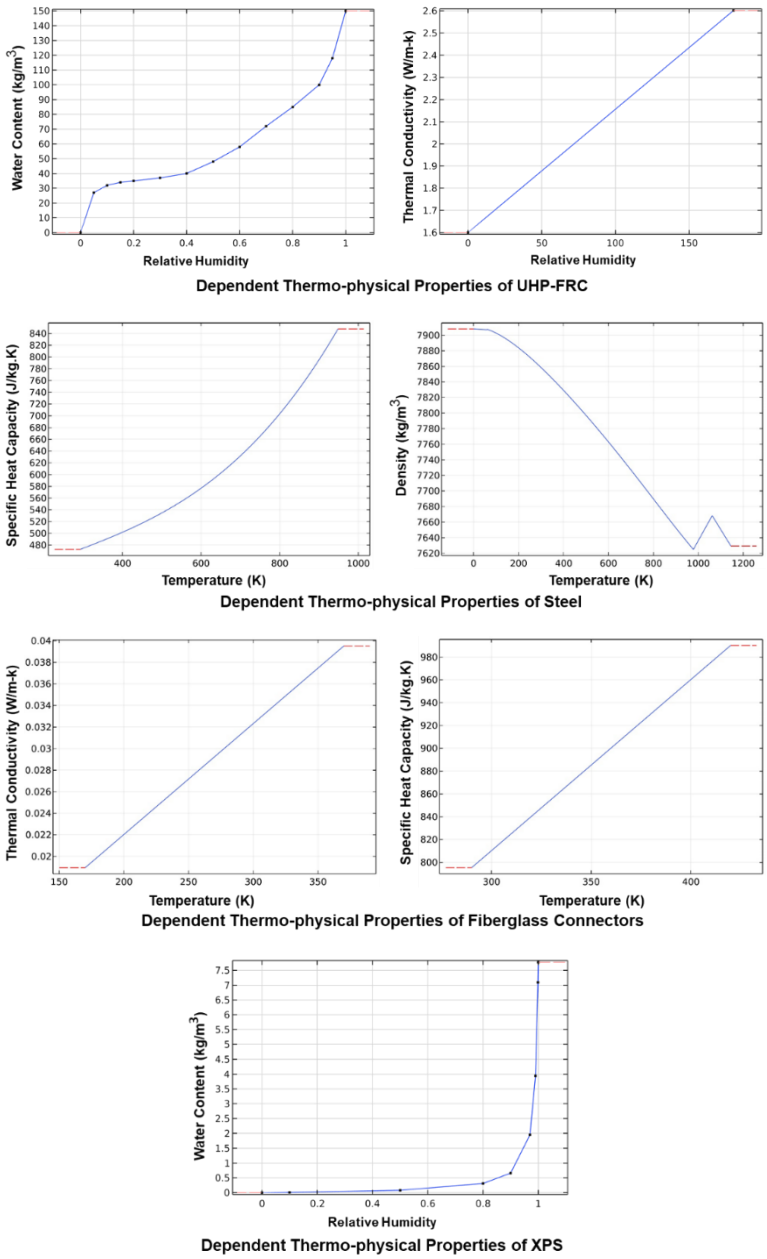

Figure 4-5 Thermos-physical properties of constituent materials of UHP-FRC panel and steel connections

4.2.3 Simulation Parameters

Non-structured and non-uniform tetrahedral meshes are generated with fine cells distributed in areas near the steel connections and fiberglass connector where potential variations in heat and moisture transfer are large in order to achieve an accurate and mesh-independent simulation while keeping the total mesh size within a reasonable number. Figure 4-6 illustrates the generated meshes for all panel connections.

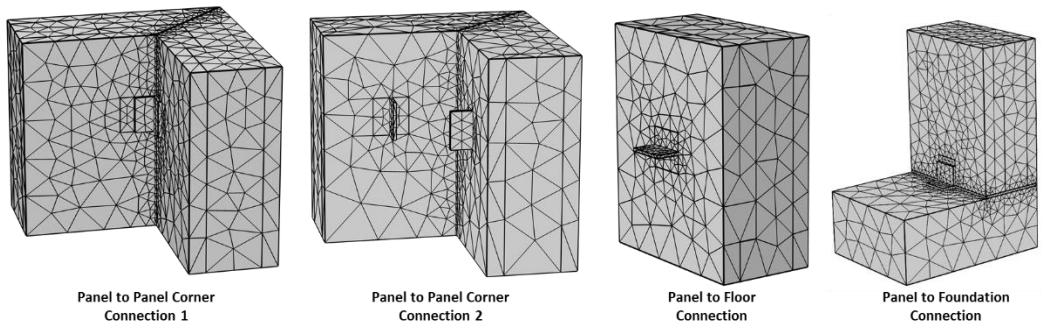

Figure 4-6 Meshes generated for panel connections

Figure 4-7 illustrates boundary conditions applied to the models. The interior surface of the models is exposed to the indoor fixed temperature of 19 °C (292.15 K) with the convective heat transfer coefficients of 5 (W/m^2K). On the other hand, the exterior surface of the models is exposed to ambient temperature and relative humidity with a combined convective and radiation-related heat

transfer coefficient of 25 (W/m^2K). Adiabatic conditions (no heat and moisture fluxes) are also applied to the remaining surface on the models.

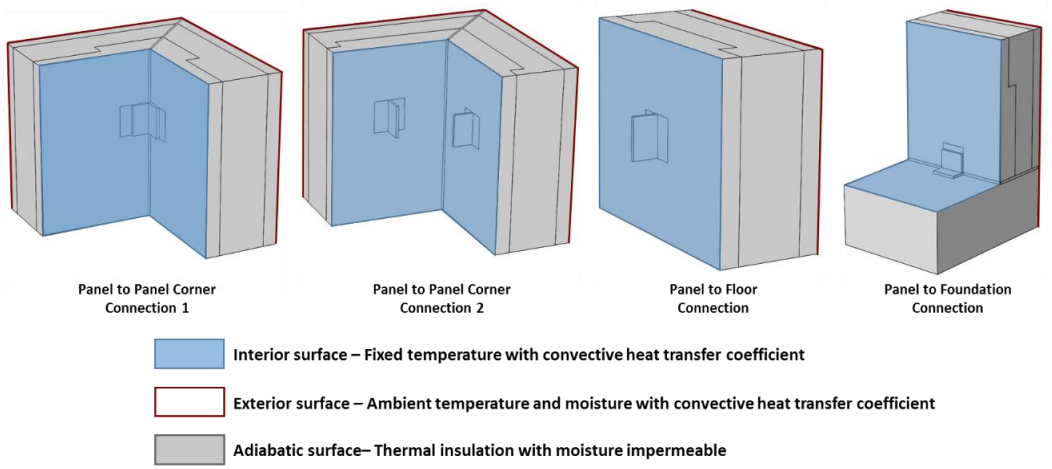

Figure 4-7 Graphical representation of boundary conditions for panel connections

The meteorological data for Miami International Airport (ASHRAE) (Roth, 2017) is used for the simulation to provide ambient temperature and relative humidity for exterior surfaces in the simulations. Simulations are conducted in June 2019 for 3 months (90 days). Figure 4-8 illustrates the ambient temperature and relative humidity used in simulations.

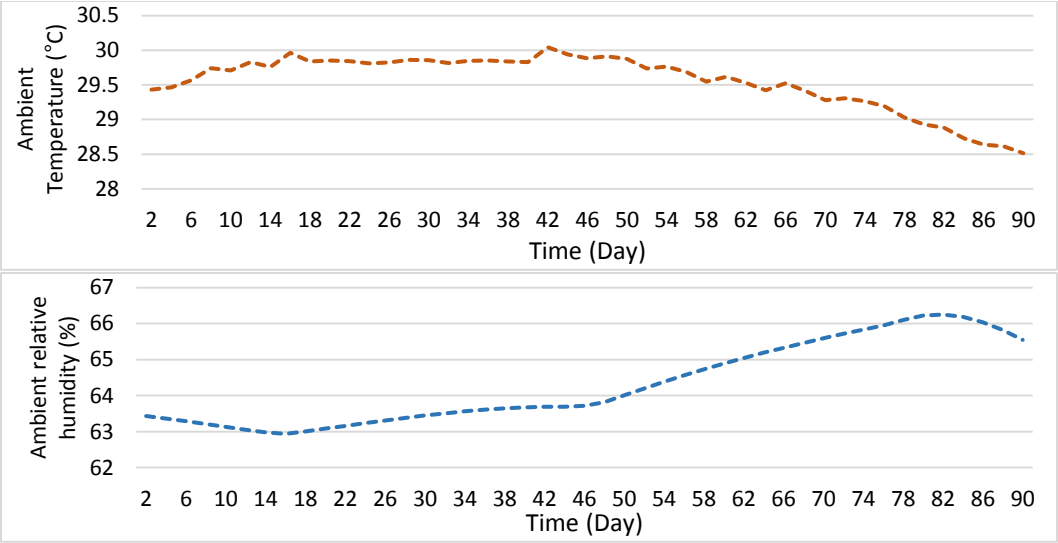

Figure 4-8 Ambient temperature and relative humidity for Miami International Airport in July 2019 for 3 months (90 days) evolution

4.3 Results and discussions

4.3.1 Results of Heat Transfer

Figure 4-9 illustrates the spatial distribution of temperature in the cross-sections of panel connections. This figure shows that the insulation layers in all cases, except for panel to foundation case, could regulate the temperature distribution within the cross-sections. Although steel connections have lower thermal resistivity compared to concrete and insulation layers, they do not interfere with the temperature distribution within these cases, since they have placed on the interior side of the insulation layer. But for the panel to foundation connection case, steel connection accelerates the heat transfer between outdoor and indoor environments, therefore the temperature of the interior structural layer increases.

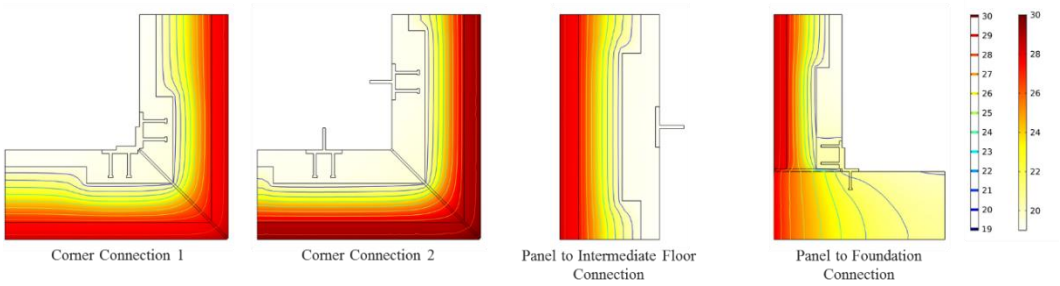

Figure 4-9 Temperature (°C) distribution within panel connections after 3 months

Figure 4-10 illustrates the heat flux magnitude within the cross-sections of panel connections. The results show that steel connections in all the cases, except panel to intermediate floor connection, have the highest heat flux magnitude within cross-sections compare to other materials. Comparing the maximum heat flux for all the cases shows that the steel connector of the panel to foundation connection has the highest heat flux among the others with 260 W/m^2 intensity. On the other hand, the heat flux in the steel connector of panel to intermediate floor connection is the least among the others with 15 W/m^2 intensity.

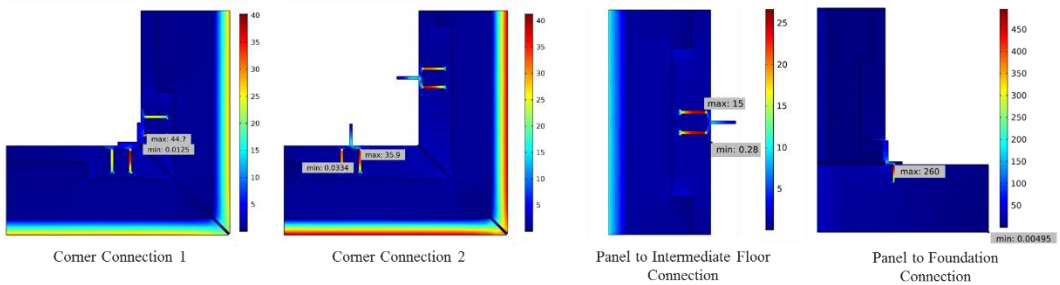

Figure 4-10 Heat flux (W/m2) intensity within the cross-section of panel connection after 3 months

Figure 4-11 illustrates the heat flux directions in the cross-section of panel connections in more detail. It is shown that the inward heat fluxes uniformly transfer from the exterior surface of panels toward the interior side of the panels. On the interior side of the insulation layer, heat flux convergence occurs in connections and studs with a high magnitude due to their high thermal conductivity. In all cases, the steel connections with the embedded plates and studs seem to accelerate heat transfer within the panel. To compare the heat flux within the steel connections in all the cases, maximum and minimum heat fluxes were recorded within the steel connections and shown in Figures 4-12 and 4-13. Figure 4-12 shows about 10 times higher maximum heat flux for the steel connection in the panel to foundation connection case compare to the other cases. On the other hand, the minimum heat flux is also higher for the steel connection in the panel to foundation connection case compare to the other cases.

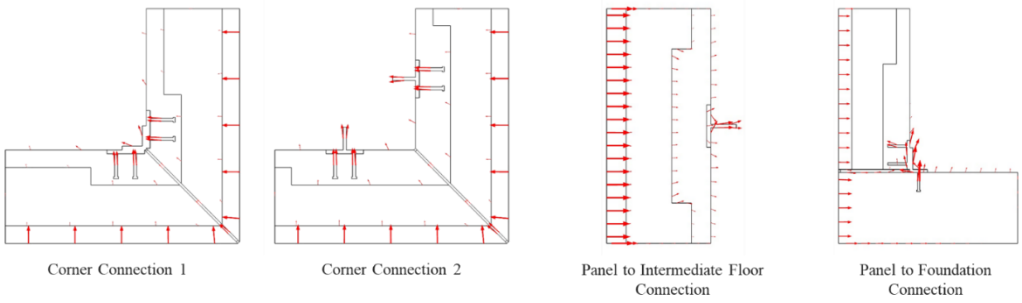

Figure 4-11 Heat flux directions within the cross-section of panel connections after 3 months

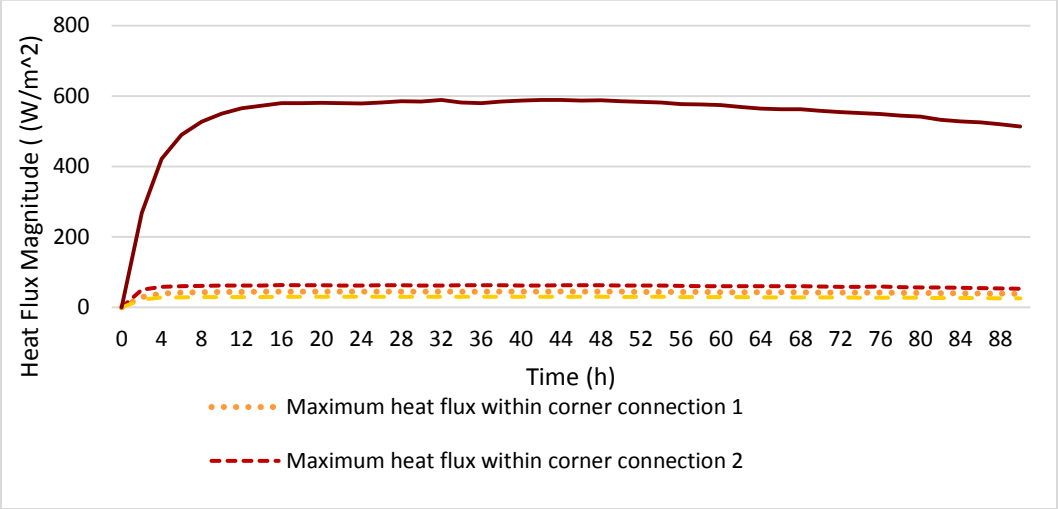

Figure 4-12 Maximum heat flux within the steel connections during 3 months

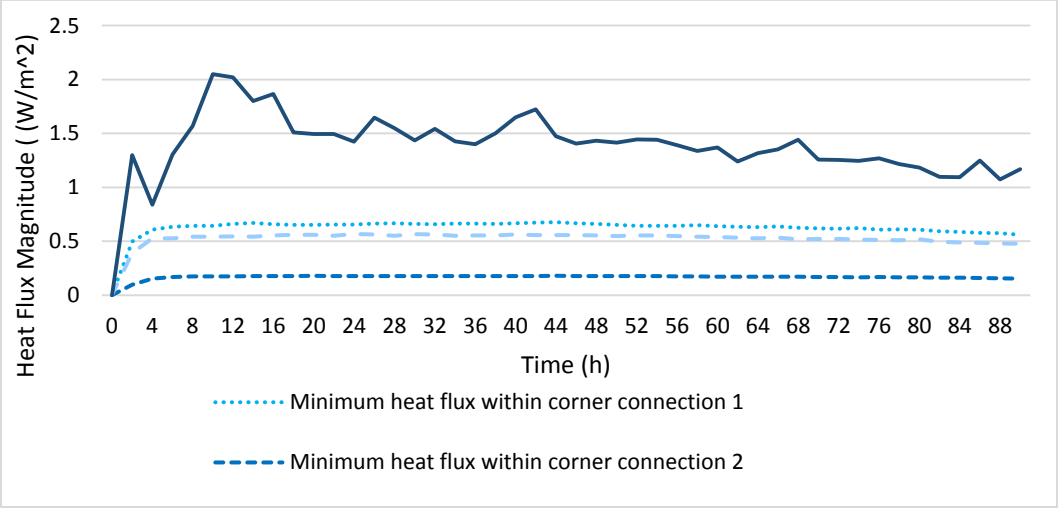

Figure 4-13 Minimum heat flux within the steel connections during 3 months

4.3.1 Results of Moisture Transfer

Although the primary reason for the investigation of moisture transfer within panel connections was to account for the effect of moisture in the heat transfer analysis, hygrothermal assessment in building multilayer porous media is essential to evaluate the risk of moisture-related problems, such as mold growth. Therefore, the detailed results of the hygrothermal assessment within panel connections are provided in this section.

Figures 4-14 and 4-15 illustrate moisture flux magnitudes and directions within the cross-section of panel connections. These figures show that the air gap layer between the panels has the highest moisture flux within both cross-sections. Figure 4-16 clearly shows that the air gap layer between the panels conducts moisture from the exterior side of the insulation layer toward the interior side since air has a lower vapor resistance factor compared to the vapor resistance factor of the insulation layer.

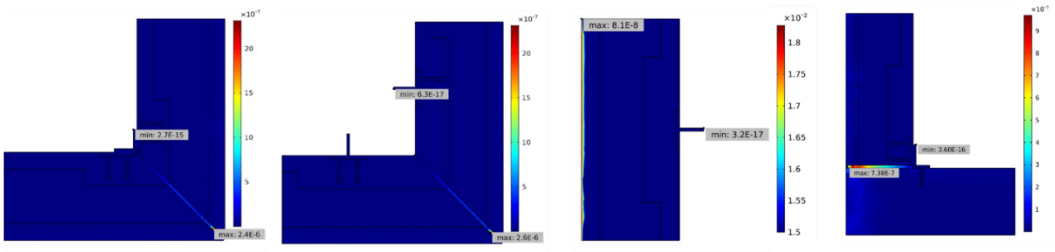

Figure 4-14 Moisture flux (kg/m^2.s) in cross-section of panel connections after 3 months

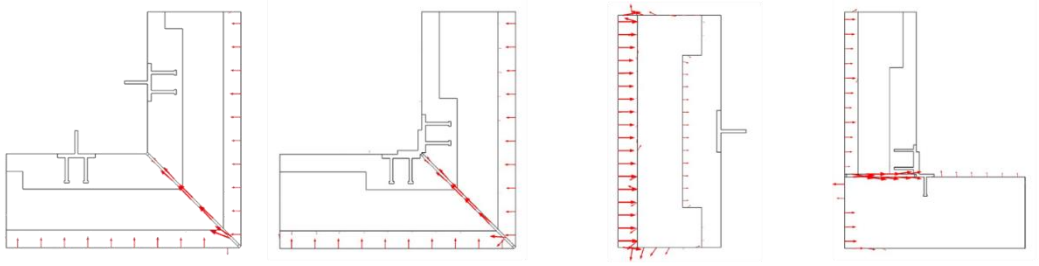

Figure 4-15 Moisture flux directions within the cross-section of panel connections after 3 months

Figures 4-16 illustrates relative humidity distribution within the cross-section of panel connections after 3 months of simulation. These figures show that the maximum relative humidity is higher on the exterior side of the insulation layer in all cases. On the other hand, the relative humidity is lower on the interior side of the insulation layer compared to the exterior side. Moreover, it seems that relative humidity fluctuates more on the exterior concrete layers compared to the interior concrete layers since the exterior concrete layers were exposed to ambient relative humidity.

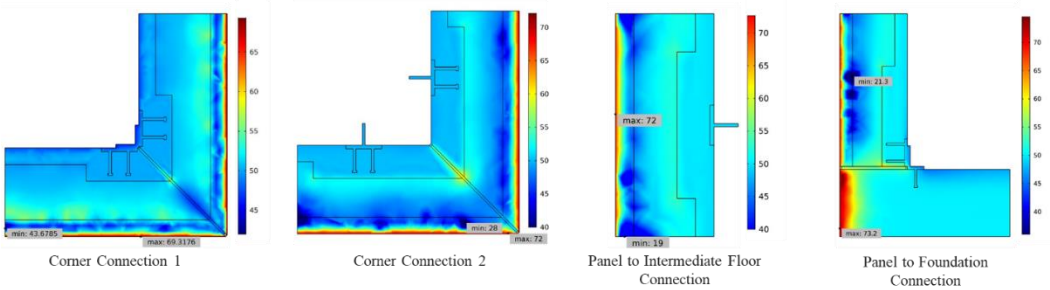

Figure 4-16 Relative humidity (%) in cross-section of panel connections after 3 months

Excessive moisture within the building materials increase the risk of mold growth (Ojanen et al., 2010). The relative humidity level of 80% for a long exposer time is considered as the lowest possible relative humidity for mold growth for very sensitive building materials, such as wood and timber. This level could be a little higher (e.g., 85%) for less sensitive materials, such as concrete and insulation material. Simulated data for temperature and relative humidity on the interior and exterior side of the insulation layer were used to evaluate the risk of mold growth within the panel in all cases. The results for all cases showed that the maximum relative humidity on both sides of the insulation layer was 49, 53, 55, and 57% for Corner Connection 1, Connection 2, panel to intermediate floor connection, and panel to foundation connection, respectively, which are considerably less than 80%. Therefore, the risk of mold growth for all cases was zero.

4.4 Conclusion

In developing innovative façade systems, energy efficiency is one of the most important criteria that has to be addressed. However, oversimplification in the analysis of complex panel connections and ignoring the hygroscopic behavior of materials can lead to either overestimation or underestimation in energy performance analysis of building façade systems. In this paper, a transient heat, air, and moisture transfer model was developed based on the conservation of mass and

energy to evaluate heat and moisture behavior within four proposed panel connections by Precast/Prestressed Concrete Institute (PCI). The coupled partial differential equations for heat and moisture transfer were simultaneously solved using a finite element method (FEM) based approach. UHP-FRC façade panel was used as a case. The simulation results showed that steel corner connections exacerbate heat loss within façade panels due to the high thermal conductivity of steel. On the other hand, the result of moisture transfer showed that moisture flux convergence happens only in air gap layers between the panels at the corner of connections. Results also showed that relative humidity fluctuates more on the exterior concrete layer of both cases compared to the interior concrete layers, but it didn't reach the lowest level of relative humidity. The results show the significant importance of connections in the energy performance analysis of façade systems. These findings contribute to the body of knowledge by highlighting the applicability of the proposed methodology to investigate the heat and moisture transfer in different building façade panel connections. It is expected that the results will be used by facade designers for further thermal investigation in façade connections.

CHAPTER 5

BUILDING ENERGY PERFORMANCE ANALYSIS OF UHP-FRC PANELS IN THE CONTEXT OF BUILDING

The building energy performance analysis of UHP-FRC and conventional panels in the context of building has been carried out through a comparative approach considering uncertainty in design and input parameters. The objective of this chapter is to investigate the combined effect of different building types and climate conditions on these panels' energy performance under uncertainty, which includes:

- Conducting probabilistic building energy performance analysis of UHP-FRC façade panels and compare with the building energy performance analysis of conventional panel as a baseline; and
- Investigating the impact of building operation schedules on the energy performance of the UHP-FRC façade panels.

5.1 Methodology

Figure 5-1 presents the process to evaluate the energy performance of the UHP-FRC façade systems in comparison with the performance of the conventional façade systems in building context. To evaluate the energy performance of UHP-FRC panels and compare it with the energy performance of conventional panels in

the context of building, fourteen U.S. Department of Energy (DOE) prototype buildings were selected to represent different building types. Thermophysical properties of façade systems in these buildings were replaced by two competing façade alternatives (conventional panels and UHP-FRC panels). Probabilistic models were created to represent the uncertainties in design input parameters in the building simulation models. The probabilistic models of the input parameters were randomly sampled using Latin Hypercube Sampling (LHS) to create a pool of randomly generated buildings (100 buildings) for each scenario. Therefore, 210 scenarios were evaluated in total. Moreover, we investigated the impact of the uncertain parameters in building operation schedules for a DOE medium office building and evaluated in three locations. Randomly generated building models were simulated using *EnergyPlus*™, a high fidelity whole building energy simulation tool developed by DOE (U.S. Department of Energy, 2016b). Finally, the results of simulations were compared for buildings with two competing façade systems. This analytical process is elaborated in the following sections.

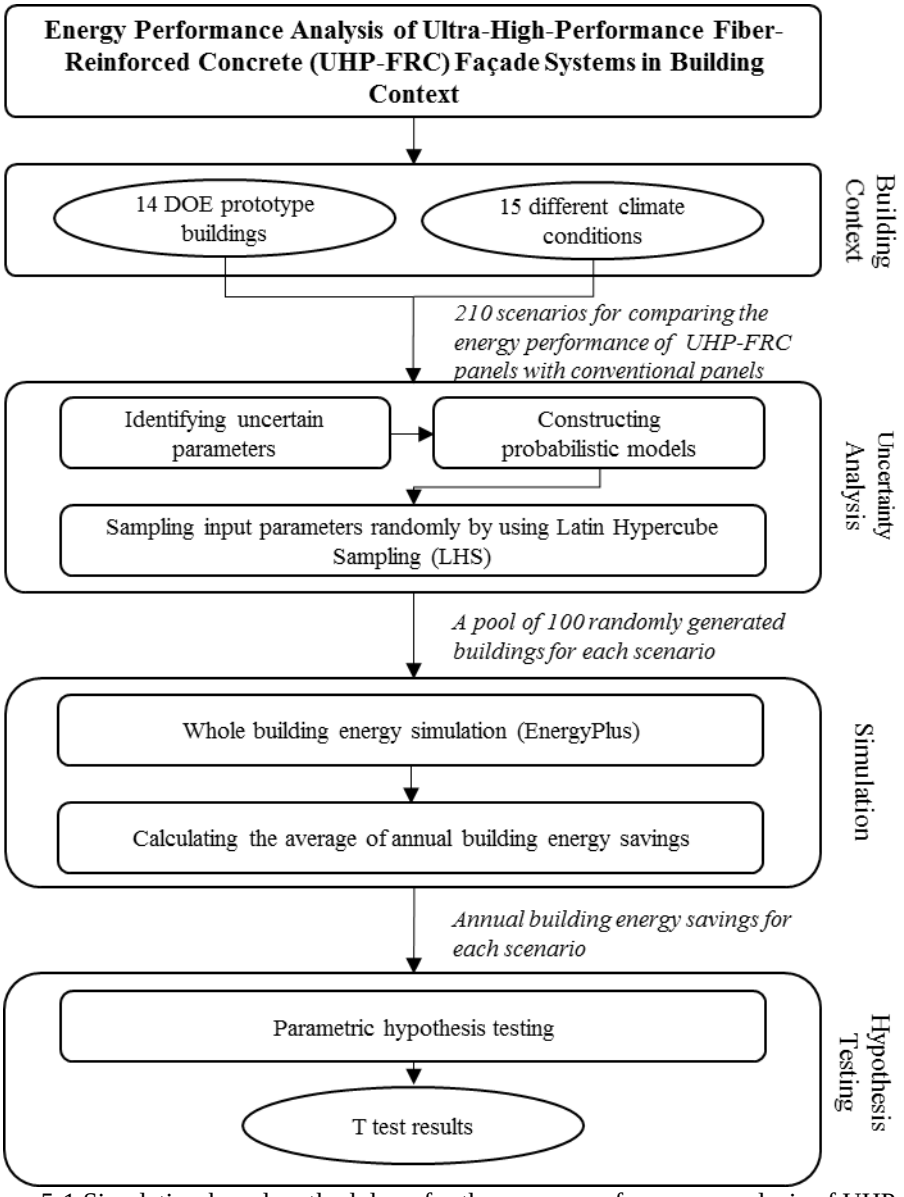

Figure 5-1 Simulation-based methodology for the energy performance analysis of UHP-FRC façade systems in building context

5.1.1 DOE Prototype Buildings

The DOE commercial prototype buildings are used to represent the building contexts to evaluate the energy performance of the UHP-FRC panel. These prototype buildings that support ANSI/ASHRAE/IES Standard 90.1 are commonly used as a consistent baseline for whole building energy simulation analysis (U.S. Department of Energy, 2016a). They collectively characterize more than 70% of the commercial building stock in the U.S. (National Renewable Energy Laboratory, 2011). Table 5-1 describes 16 DOE prototype buildings. Figure 5-2 shows the 3D model of DOE prototype buildings.

Table 5-1 Description of DOE prototype buildings

Buildings	Total Floor Area*	Window Fraction	Number of Floors	Aspect Ratio	Cooling system	Heating system	Roof construction
High-rise Apartment	84360	0.3	10	2.75	Water heat pumps	Water heat pumps	Built-up Roof
Mid-rise Apartment	33700	0.2	4	2.74	Split system DX	Gas furnace	Built-up Roof
Large Hotel	122132	0.302	7	5.07	Air-cooled chiller	Gas-fired boiler	Insulation above Deck
Small Hotel	43200	0.109	4	3	PTAC, Split system	PTAC, Gas furnace	Built-up Roof
Primary School	73960	0.35	1	1.3	Packaged air conditioning	Gas furnace	Built-up Roof
Secondary School	210900	0.33	2	1.4	Air conditioner, Air-cooled Chiller	Gas furnace	Built-up Roof
Fast Food Restaurant	2500	0.14	1	1	Packaged air conditioning	Gas furnace	Unconditioned attic roof
Strip Mall Retail	22500	0.105	1	4	Packaged air conditioning	Gas furnace	Built-up Roof
Standalone Retail	24695	0.071	1	1.28	Packaged air conditioning	Gas furnace	Built-up Roof
Warehouse	49495	0.0071	1	2.2	Packaged air conditioning	Gas furnace	Metal Building Roof
Small Office	5500	0.21	1	1.5	Air-source heat pump	Air-source heat pump	Attic roof with wood joist
Medium Office	53600	0.33	3	1.5	Packaged air conditioning	Gas furnace	Built-up roof
Large Office	498600	0.4	13	1.5	cooling coil and centrifugal chillers	Gas-fired boiler	Built-up Roof
Hospital	241410	0.16	6	1.31	Chillers	Gas boiler	Built-up Roof

*Square feet

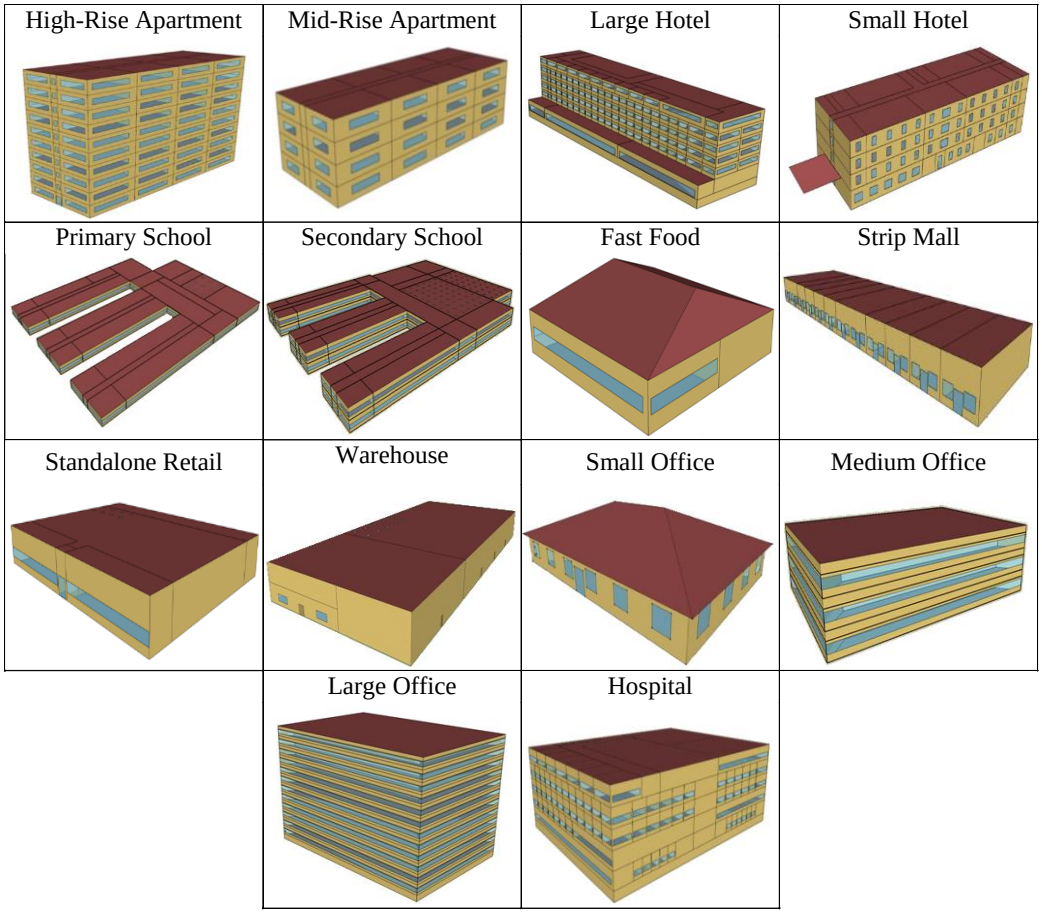

Figure 5-2 3D model of DOE prototype buildings

Thermophysical properties of facades in the building prototypes were replaced in EnergyPlus models to reflect two competing façade alternatives: conventional panels and UHP-FRC panels. The structural and insulation layers in these two façade systems have different thermophysical properties. UHP-FRC layer has a higher specific heat and density compared to the conventional concrete layer. However, its conductivity is less than conventional concrete.

5.1.2 DOE Climate Zones and Representative Cities

The DOE climate zones are used to represent the climate conditions to evaluate the energy performance of the UHP-FRC panel. DOE climate zones were developed based on Solar and Meteorological Surface Observation Network (SAMSON) weather data to provide consistent climate materials for all compliance methods and code sections for DOE and ASHRAE Standard 90.1-2004 (Briggs et al., 2003). This classification divides the country into three bands from east to west (moist, dry, and marine) and eight subdivisions from south to north (1 to 8). Table 5-2 provides characteristics of typical locations (cities) in each climate zone.

Table 5-2 Characteristics of DOE climate zones representativeness cities (Adopted from U.S. Department of Energy, 2018b)

City	Climate Zone	Climate Zone Name and Type	Annual Air Dry Bulb Temperature (°C)			Extreme Annual Dry Bulb (°C)		Extreme Wet Bulb (°C)	Wind Speed (m/s)*		
			Average	Min	Max	Min	Max		1%	2.50%	5%
Fairbanks	8	Sub-Arctic	-1.4	-19.3	16.9	-3.6	38.1	22.4	7.7	6.7	5.5
Duluth	7	Very Cold	4.0	-13.0	17.8	-31.3	32.0	26.5	11.1	9.4	8.6
Helena	6B	Cool-Dry	7.2	-5.0	20.5	-29.1	37.0	24.8	10.9	9.2	8.2
Burlington	6A	Cool-Humid	7.9	-7.2	21.1	-25.8	34.0	27.9	10.6	9.1	8.2
Chicago	5A	Cool-Humid	10.0	-4.6	24.1	-22.2	35.6	28.5	11.0	9.4	8.5
Boise	5B	Cool-Dry	11.2	-1.7	24.5	-15.8	40.1	22.8	9.8	8.5	7.6
Albuquerque	4B	Mixed-Dry	13.7	2.1	25.6	-11.7	37.5	21.4	12.6	11.1	9.2
San Francisco	3C	Warm-Marine	13.8	9.6	16.7	1.9	34.4	22.3	12.8	11.5	10.5
Salem McNary	4C	Mixed-Marine	11.7	4.6	20.1	-8.2	37.7	26.8	9.3	8.2	7.3
Baltimore	4A	Mixed-Humid	13.2	-0.5	25.3	-13.9	36.8	29.2	10.0	8.5	7.6
Memphis	3A	Warm-Humid	17.0	4.1	28.3	-10.8	37.4	29.4	9.0	8.1	7.4
El Paso	3B	Warm-Dry	18.0	6.8	27.9	-8.2	40.7	23.8	11.8	10.0	8.4
Houston	2A	Hot-Humid	20.4	10.5	28.3	-3.6	38.1	28.8	8.8	7.9	7.3
Phoenix	2B	Hot-Dry	23.8	11.7	35.6	1.2	45.9	27.7	8.3	7.2	5.8
Miami	1A	Very Hot-Humid	24.5	19.4	28.1	5.3	35.0	29.3	9.1	8.3	7.6

*Percentages indicate the annual cumulative frequency of occurrence.

5.1.3 Uncertainty Analysis

Uncertainty limits the confidence of building energy simulation results (Moon, 2005; Eisenhower et al., 2012), which may lead to a significant discrepancy between the simulation results and actual building energy consumptions.

Buildings are complex systems, characterized by multiple parameters, such as design geometry, material properties, occupancy levels, equipment schedules and operations, and climate and weather conditions (Coakley et al., 2014). Diverse sources of uncertainty originate from these parameters. De Wit and Augenbroe (2002) classified these uncertain parameters into four categories: 1) specification uncertainty; 2) modeling uncertainty, which is mostly due to the simplifications and assumptions in the building models; 3) numerical uncertainty; and 4) scenario uncertainty. A number of studies have been conducted to identify and quantify the impact of the above-mentioned uncertain parameters on building energy performance simulation outputs. In a comprehensive study, Eisenhower et al. (2012) conducted an uncertainty analysis to screen the most critical uncertain parameters in a building model. The authors considered more than 1000 uncertain parameters in the building energy performance process. They varied all nonzero parameters about 20% of their nominal values using uniform distribution and those with zero nominal value using exponential distribution. The authors performed a decomposition to quantify which subsystems have the most impact on the building

energy uses. They found that cooling and heating setpoints are critical uncertain parameters in terms of building heating and cooling loads. Moreover, occupancy and lighting schedules are dominating parameters in terms of zone internal loads.

Hopfe (2009) found that the heat conductivity of external wall components, equipment heat gains, and infiltration rate are the most critical uncertain parameters that are needed to be considered in the energy performance evaluation. In another research, Hopfe and Hensen (2011) considered physical properties and weather conditions as uncertain parameters and used them for supporting decision making in different climate conditions. In similar studies, occupancy level, indoor design condition, lighting loads, and weather-related uncertainties were recognized as critical parameters affecting the amount of building energy uses (Hopfe et al., 2007; Lam et al., 2008; Guerra-Santin and Itard, 2010; Sun et al., 2011; Bhandari et al., 2012; Li et al., 2015; Soto et al., 2015; Berkeley et al., 2015; and Menberg et al., 2016).

de Wit and Augenbroe (2002) emphasized on quantified model uncertainties using expert judgments where the uncertainty cannot be estimated using statistical methods. They found that the combination of expert judgment and statistical methods shows promising outputs in quantifying the impact of uncertainties in building energy models.

In this paper, two major sources of uncertainty are considered in the energy performance analysis of UHP-FRC façade panels: uncertainty in design input parameters and uncertainty in building operation schedule.

5.1.3.1 Uncertainties in design input parameters

To consider the impact of uncertainties in the energy performance analysis of UHP-FRC façade panels, three critical input parameters of the simulation models were selected due to their highly acknowledged importance in the literature of probabilistic building energy performance analysis: infiltration rate, occupancy level, and lighting loads (Hopfe et al., 2007; Li et al., 2015; Soto et al., 2015, Berkeley et al., 2015; and Menberg et al., 2016). Since the objective of this study is the energy performance evaluation of two competing façade systems, the uncertainties in thermo-physical properties of different layers of these facade systems were also taken into account. Probabilistic models were created to represent uncertainties of critical input parameters. Table 5-3 shows the recommended probability distributions, mean values, and standard deviations in the literature that we used to model the uncertain parameters.

Table 5-3 Uncertain parameters and their probability distributions

Uncertain parameters	Distribution	Distribution parameters		References
		Conventional panel	**UHP-FRC panel**	
Insulation conductivity	Normal	μ=0.0058, σ=0.0023	μ=0.0058, σ= 0.0023	Lomas and Eppel, 1992; Hopfe et al., 2007; Petr et al., 2007; Lee et al., 2013; Bhamornsiri et al., 2013; Li et al., 2015; Dhariwal and Banerjee, 2015; Soto and Jentsch, 2015.
Insulation specific Heat	Normal	μ=645, σ=38.7	μ=645, σ=38.7	
Insulation density	Normal	μ=28, σ=5.3	μ=20, σ=3.78	
Concrete conductivity	Normal	μ=2.31, σ=0.13	μ=1.77, σ=0.1	
Concrete specific Heat	Normal	μ=832, σ=49.9	μ=1010, σ=60.6	
Concrete density	Normal	μ=2322, σ=441	μ=2403, σ=456	
Infiltration rate	Normal	μ=0.21, σ=0.014	μ=0.21, σ=0.014	
Occupancy level	Triangle	a=1, c=2.5, b=5.2	a=1, c=2.5, b=5.2	
Lighting level	Uniform	a=0.01, b=5	a=0.01, b=5	

Latin hypercube sampling (LHS) was used to explore the input space of uncertain parameters effectively. Latin hypercube sampling (LHS) is an updated Monte Carlo technique for sampling (McKay et al., 1979), which has become a popular technique due to its simplicity, efficiency, ease of implementation, and reasonable computational cost (Helton and Davis 2003). A hundred iterations were sampled to create pools of randomly generated buildings. This number of iterations was selected to achieve valid results, which is higher than the recommended iteration numbers (80 iterations) by Macdonald (2002).

5.1.3.2 Uncertainties in building operation schedules

One of the critical parameters affecting building energy consumptions is building operation practices (Wang et al., 2012). Maintaining the indoor thermal comfort level in buildings with various operation schedules may result in different building energy uses. Two levels of practice – good and poor – in building operations were selected and simulated in the DOE medium office prototype building for all fifteen locations. Table 5-4 presents the range of good and poor practices for the selected building operation parameters in the medium office building (Wang et al., 2012).

Table 5-4 Range of building operation parameters in good and poor practice (Wang et al., 2012)

Operation parameters	Poor practice	Good practice
Lighting control	Manual switch on/off	Dimming based on occupancy sensors and illuminance set point
Plug-in equipment control	No energy saving measures	Turn off when occupants leave
Room temperature set point for occupied hours	22 °C for heating; 23 °C for cooling	20 °C for heating; 25 °C for cooling
Minimum flow settings VAV box	50% of the design flow rate	15% of the design flow rate
Night setbacks	18.3 °C for heating set point and 26.7 °C for cooling set point for unoccupied hours	12.7 °C for heating set point and 30 °C for cooling set point for unoccupied hours

5.1.3.3 Whole Building Energy Simulations

Whole building energy simulations were used to compute the energy consumptions of the randomly generated buildings. Whole building energy simulations can be used for evaluating the performance of the building's façade, HVAC, lighting, water, and control systems (Crawley et al., 2000). In the last decades, several studies have been done a variety of building energy simulation programs have been developed to estimate future energy use of the buildings by simulating the complex interactions within buildings (Parent, 2002), such as BLAST, DOE-2.1E, ECOTECT, eQUEST, and EnergyPlus. Among all these building energy performance simulation tools, EnergyPlus has gained more attention in the United States. Researchers and practitioners widely use EnergyPlus for estimating building energy performance in the academic and building communities because as a stand-alone whole building energy simulation tool, it models hourly energy use of buildings and gives the opportunity of manipulating construction, internal loads, schedules, and even weather by the modelers (Sailor, 2008). In this research, EnergyPlus was used to simulate the building energy use of buildings with UHP-FRC and conventional panels in 210 different scenarios. All building types listed in Table 3 were simulated in 15 climate zones using weather data (.epw files) available for each representative city. The simulation results were used to compare the performance of the UHP-FRC panel with the conventional panel.

In another set of assessments, building energy simulations were performed to analyze the impact of insulation material on the energy performance of UHP-FRC façade panel. In this set, the UHP-FRC insulation layer was changed to EPS layer, and its energy performance was compared with the conventional panel in a DOE medium office building under the same uncertain parameters.

5.1.3.4 Hypothesis Testing

It is critical to test whether the simulation results contain enough information to conclude that using UHP-FRC panel reduces the building energy consumptions compared with the conventional panel. Therefore, hypothesis testing was used to consider the combined mean and standard deviation in the comparison of both panels' energy performance. The simulated energy consumptions for each scenario were used to test the hypothesis that the average of annual energy consumptions of the randomly generated prototype buildings with the UHP-FRC façade panel is less than the average of annual energy consumption of the prototype building with conventional Panel. The t-test was used to evaluate this hypothesis. The null hypothesis of this test is that the average of annual energy consumption of the randomly generated DOE prototype buildings with the UHP-FRC façade panel is equal or higher than annual energy consumption of the buildings with the

conventional Panel. Rejection of the null hypothesis provides us with enough evidence to suggest that using UHP-FRC panels results in energy savings.

5.2 Results and Discussion

5.2.1 Results of Whole Building Energy Simulation

The outputs of building energy simulations were used to compare the energy performance of buildings enhanced by UHP-FRC façade panels with the baseline buildings with the conventional façade panels. Table 5-5 illustrates the average annual building energy savings for different scenarios when the conventional panels are being replaced with the UHP-FRC panels. Based on these results, replacing the conventional panels by the UHP-FRC panels reduces the building energy consumptions in 203 scenarios out of 210; only in seven scenarios, the energy savings were negative. The small office prototype building in Fairbanks showed the highest energy savings (5.64%). The warehouse in El Paso showed the lowest energy savings (-1.72%). The absolute values of the remaining six negative energy savings are smaller than 1.

Table 5-5 The average annual building energy savings by replacing the conventional panel with UHP-FRC panel

Representative cities in each climate zone / Buildings	Fairbanks	Duluth	Helena	Burlington	Chicago	Boise	Albuquerque	San Francisco	Salem McNary	Baltimore	Memphis	El Paso	Houston	Phoenix	Miami
Mid-rise apartment	4.44%	3.40%	4.44%	3.48%	3.22%	3.87%	2.12%	-0.05%	3.45%	2.78%	2.26%	1.31%	1.15%	1.87%	1.39%
High-rise apartment	3.85%	3.25%	4.19%	3.33%	3.13%	3.78%	1.54%	0.88%	3.56%	2.82%	1.97%	5.06%	1.08%	1.47%	0.98%
Small hotel	3.22%	2.52%	2.81%	2.42%	2.27%	2.36%	1.51%	0.20%	1.86%	1.81%	1.41%	1.15%	0.96%	1.52%	1.43%
Large hotel	1.85%	1.91%	1.57%	1.63%	1.35%	1.04%	0.40%	0.07%	0.92%	0.76%	0.42%	0.12%	0.12%	0.30%	0.08%
Primary school	2.21%	1.17%	0.62%	0.90%	0.89%	0.33%	0.19%	-0.13%	0.09%	0.38%	0.37%	0.22%	0.36%	0.87%	0.55%
Secondary school	1.23%	0.80%	0.86%	0.78%	0.69%	0.60%	0.10%	0.02%	0.38%	0.41%	0.14%	0.06%	-0.02%	0.42%	0.10%
Fast food restaurant	0.15%	0.15%	0.09%	0.14%	0.15%	0.12%	0.05%	0.14%	0.10%	0.15%	0.25%	0.29%	0.30%	0.24%	0.52%
Strip mall retail	1.62%	1.38%	1.39%	1.27%	1.25%	1.19%	0.99%	0.08%	1.15%	1.00%	0.96%	0.57%	0.93%	0.96%	1.09%
Standalone retail	1.83%	1.45%	1.41%	1.35%	1.33%	1.09%	0.54%	-0.87%	0.95%	1.00%	0.95%	0.38%	0.70%	1.07%	1.35%
Warehouse	2.23%	1.47%	0.89%	1.23%	1.10%	4.28%	0.81%	2.26%	0.01%	0.36%	3.66%	-1.72%	1.86%	-0.04%	2.82%
Small office	5.64%	4.23%	3.53%	3.62%	3.23%	2.59%	1.19%	-0.08%	2.37%	2.15%	1.43%	1.00%	0.81%	1.49%	1.07%
Medium office	1.81%	1.37%	1.20%	1.16%	1.18%	0.98%	0.64%	0.24%	1.11%	0.89%	0.79%	0.48%	0.60%	0.99%	1.38%
Large office	1.69%	1.51%	1.72%	1.62%	1.51%	1.40%	0.71%	0.35%	1.47%	1.04%	0.77%	0.32%	0.31%	0.34%	0.26%
Hospital	2.49%	2.52%	2.54%	2.28%	2.32%	2.47%	1.86%	2.03%	2.50%	1.93%	1.85%	1.82%	1.47%	1.44%	1.04%

The results show that average annual energy savings are positive for eight prototype buildings (high-rise apartment, small hotel, hospital, large hotel, large office, medium office, fast-food restaurant, retail strip mall, and small hotel) in all locations. The energy savings are positive for all the building types in eleven locations (Fairbanks, Duluth, Helena, Burlington, Chicago, Boise, Albuquerque, Baltimore, Memphis, and Miami). On average, savings are higher in cold climates (e.g., Fairbanks) than savings in temperate climates (e.g., San Francisco). This is because a tighter building construction using UHP-FRC panels needs heating or cooling during the transition seasons (spring and fall) in the temperate climates.

Also, on average, buildings that are dominated by internal loads (e.g., fast food restaurant where all energy savings are within 1 percent) seem to benefit the least from UHP-FRC. Buildings can be classified as 'internally-dominated' buildings such as large office buildings and 'envelope-dominated' buildings such as smaller buildings with higher surface area to volume ratio (Lechner, 2014). The energy use of internally-dominated buildings, which are also more schedule-driven are more impacted by their internal load (e.g., people, equipment, etc.) than their envelope. In other words, the climate has less impact on internally-dominated buildings than envelope-dominated buildings. As a result, an internally-dominated building is also less impacted by the conductivity of its envelope.

The results in Table 5-6 show that replacing the conventional panels by the UHP-FRC panels reduces the building energy consumptions in most of the scenarios. However, the average energy savings for some of the scenarios seem to be extremely small. Figure 5-3 shows the boxplots of annual energy consumptions of mid-rise apartments with both UHP-FRC and conventional façade panels in 15 locations. This figure shows the distribution of energy consumptions in buildings with UHP-FRC and conventional façade panels based on six statistical parameters: minimum, first quartile, median, third quartile, maximum, and mean values. Even though the average energy consumption of buildings with UHP-FRC façade panels is lower than the average energy consumption of buildings with conventional façade panels for all the scenarios, the differences between the statistical parameters

for energy consumptions of buildings with both UHP-FRC and conventional façade panels are too small in each scenario. The higher overlap between two box-plots indicates the lower chance of significant difference between the energy savings. Therefore, the hypothesis testing was conducted for all the scenarios to test whether the energy savings are significant with considering both mean and standard deviation values.

Table 5-6 Descriptive statistics of annual energy use for mid-rise apartments with UHP-FRC and conventional façade panels

Locations	Panel type	Mean	Standard deviation	Maximum	Minimum
Albuquerque	Conventional	626.1	13.8	657.3	586.8
	UHP-FRC	616.9	13.0	652.6	584.7
Vancouver	Conventional	649.9	53.4	786.0	512.8
	UHP-FRC	620.4	47.4	722.7	518.9
Baltimore	Conventional	979.3	36.0	1096.9	890.3
	UHP-FRC	952.9	38.9	1080.9	879.9
Boise	Conventional	743.4	34.7	864.4	662.3
	UHP-FRC	716.8	35.2	828.8	655.7
Burlington	Conventional	1513.3	78.6	1697.1	1304.6
	UHP-FRC	1461.9	73.5	1689.4	1320.6
Chicago	Conventional	1445.9	61.9	1634.9	1294.5
	UHP-FRC	1402.9	67.7	1612.7	1271.1
Duluth	Conventional	2074.8	105.5	2320.1	1791.0
	UHP-FRC	2005.7	98.1	2304.1	1811.3
El Paso	Conventional	729.5	30.8	798.2	672.7
	UHP-FRC	714.2	80.2	821.4	656.9
Fairbanks	Conventional	2565.0	109.0	2817.3	2225.8
	UHP-FRC	2467.1	87.4	2656.9	2282.5
Helena	Conventional	900.8	56.5	1043.6	748.9
	UHP-FRC	863.6	48.0	970.1	762.8
Houston	Conventional	878.0	29.0	936.8	823.6
	UHP-FRC	868.8	29.3	962.3	802.7
Memphis	Conventional	925.7	22.1	978.5	869.0
	UHP-FRC	907.8	16.8	961.0	856.1
Miami	Conventional	1233.5	43.8	1317.7	1144.6
	UHP-FRC	1221.5	43.7	1349.8	1120.1
Phoenix	Conventional	964.8	950.7	1032.9	894.8
	UHP-FRC	35.6	35.5	1057.5	871.2
Riyadh	Conventional	1015.6	35.8	1083.0	945.7
	UHP-FRC	1000.6	35.3	1107.1	918.2
Salem McNary	Conventional	584.3	34.2	678.5	511.3
	UHP-FRC	558.1	64.3	633.5	506.3
San Francisco	Conventional	160.0	20.8	225.4	130.4
	UHP-FRC	161.6	22.8	236.9	128.0

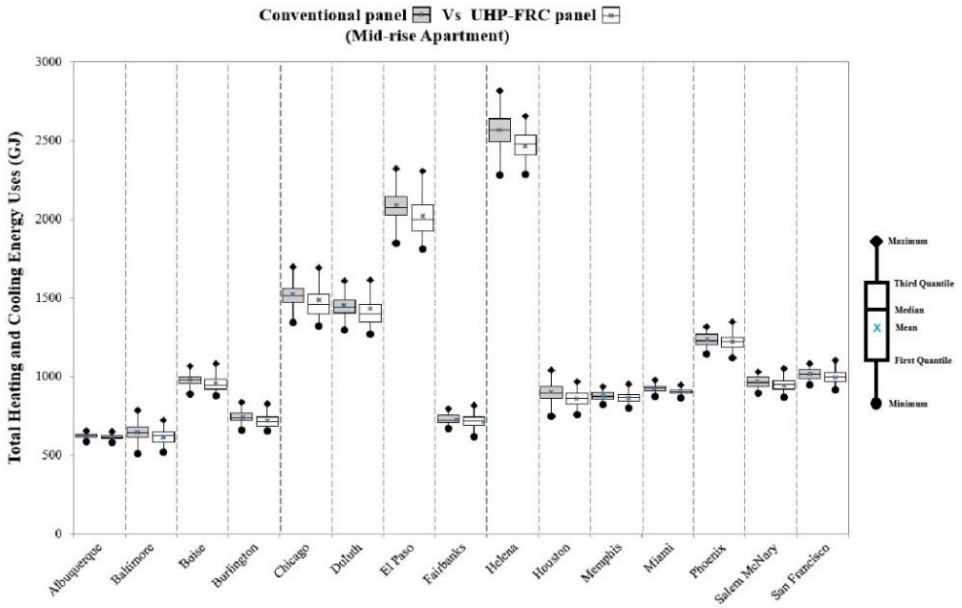

Figure 5-3 Box plots of annual energy use for mid-rise apartments with UHP-FRC and conventional façade panels

UHP-FRC façade panels reduce thermal bridging and hence reduce thermal conductivity. The temperature difference between indoor and outdoor air temperatures are usually higher in colder climates within the U.S. climate zones. For example, temperatures may drop as low as -50 °F in winter time in colder climates. That is about 80 degree difference from comfort levels. However, in warmer climates, the highest temperatures recorded are about 125 °F, which is about 50 °F from comfort ranges. Considering simple conduction heat flow equation q=U(Tin -Tout), one can see that if the temperature difference increases, heat flow also increases. Reducing thermal conductivity can help reduce heat flow when the temperature difference between indoors and outdoors increases. The same

equation explains why buildings with lower internal loads also benefit more from UHP-FRC. Such buildings are more impacted by climate and weather changes (i.e., higher heat flow) because the internal temperature is not affected by the internal loads and therefore reducing conductivity helps to save more energy in such buildings.

5.2.2 Impact of building operation schedules on the energy performance of UHP-FRC façade panels

Table 5-7 shows the percentages for energy savings of the DOE medium office building with both good and poor operational schedules when the conventional façade system is being replaced with the UHP-FRC façade system. The results show that the UHP-FRC façade panel has higher energy performance when the building is being operated based on poor practices. On the other hand, the energy savings with UHP-FRC façade panels seem to be small in good practice. Moreover, the results show that the energy savings percentages are higher in locations with cold climate conditions. In contrast, operation schedules have a lower impact on the energy performance of UHP-FRC façade panels in locations with warm and moist climate conditions such as Miami.

Table 5-7 The average annual medium office building energy savings by replacing the conventional panel with the UHP-FRC panel in good and poor operation practices

Operation \ Locations	Fairbanks	San Francisco	Miami
Good practice	0.19%	0.13%	0.04%
Poor practice	3.47%	1.77%	0.76%

5.2.3 T-test results

The results of t-test for all scenarios show that the null hypothesis (the average of annual energy consumption of buildings with UHP-FRC panels was higher than the average of annual energy consumption of buildings with the conventional Panels) was rejected for 133 scenarios at 5% level of significance (Table 5-8). For the remaining scenarios, hypothesis testing was conducted to determine whether there is enough information to support that the buildings with the conventional panels outperform the buildings with the UHP-FRC façade panels. In the 76 scenarios, the buildings with UHP-FRC façade panels perform similarly to the buildings with conventional panels. Only in one scenario (warehouse in El Paso), the results of hypothesis testing showed that the buildings with the conventional panels outperform the buildings with the UHP-FRC façade panels. The results of hypothesis testing supported the conclusion that savings are more significant in cold climates (e.g., Fairbanks) than savings in temperate climates (e.g., San Francisco). The hospital prototype building is the only building type that

showed a significant reduction in building energy use in all locations by replacing the conventional panels with UHP-FRC panels.

Table 5-8 T-test results

Representative cities in each climate zone / Buildings	Fairbanks	Duluth	Helena	Burlington	Chicago	Boise	Albuquerque	San Francisco	Salem McNary	Baltimore	Memphis	El Paso	Houston	Phoenix	Miami
Mid-rise apartment	✓	✓	✓	✓	✓	✓	✓	=	✓	✓	✓	✓	✓	✓	✓
High-rise apartment	✓	✓	✓	✓	✓	✓	✓	=	✓	✓	✓	✓	✓	✓	✓
Small hotel	✓	✓	✓	✓	✓	✓	✓	=	✓	✓	✓	✓	✓	✓	✓
Large hotel	✓	✓	✓	✓	✓	✓	✓	=	✓	✓	✓	=	=	=	=
Primary school	✓	✓	=	✓	✓	=	=	=	=	=	✓	=	✓	✓	=
Secondary school	✓	✓	=	=	=	=	=	=	=	=	=	=	=	=	=
Fast food restaurant	✓	✓	=	✓	✓	=	=	=	=	=	✓	=	✓	✓	=
Strip mall retail	✓	✓	✓	✓	✓	✓	=	=	✓	=	✓	=	✓	✓	=
Standalone retail	✓	✓	=	✓	✓	=	=	=	=	=	✓	=	✓	✓	=
Warehouse	✓	✓	✓	✓	✓	✓	=	=	=	✓	✓	×	=	=	=
Small office	✓	✓	✓	✓	✓	✓	✓	=	✓	✓	✓	=	=	✓	=
Medium office	✓	=	=	=	=	=	=	=	=	=	✓	=	✓	✓	✓
Large office	✓	✓	=	✓	✓	=	=	=	✓	✓	✓	=	✓	✓	=
Hospital	✓	✓	✓	✓	✓	✓	✓	✓	✓	✓	✓	✓	✓	✓	✓

Note: ✓, =, and × mean that the average of the annual heating and cooling energy uses of the randomly generated buildings with the UHP-FRC panel is less than, equal to, or more than the average of the annual heating and cooling energy uses of the buildings with the conventional panel, respectively (5% significance level).

Moreover, the results of hypothesis testing for the annual energy savings of buildings enhanced by UHP-FRC panels showed that there is no significant difference between using XPS and EPS insulation layers in the panels. The results show that the thicknesses and materials of different layers of panels and more

importantly structural rebars in the conventional panel cause the difference in energy performances of UHP-FRC and conventional panels.

CHAPTER 6

KNOWLEDGE DISCOVERY AND RULE EXTRACTION FROM UHP-FRC FAÇADE PANELS' SIMULATED ENERGY PERFORMANCE DATA

A building façade system plays a critical role in building energy conservation since it has a large impact on the heat transfer between the outdoor and indoor environments. Considering complex interactions between building façade design parameters and building context is essential for evaluating the energy performance of building façade systems. Building energy simulations (BESs) can help designers to acquire necessary information about the energy performance of façade systems. However, many design firms do not have the capability of performance-based design due to the lack of trained personnel and technical resources, such as simulation tools and devices. Even with all the required resources, it is computationally expensive to analyze different façade design alternatives to compare their energy performance. The main objective of this chapter is to develop a data-driven framework to extract hidden information and underlying structure from the thermal behavior of façade systems in a set of scenarios and provide recommendations for designers to select energy-efficient façade systems. In the proposed framework, clustering analysis was used to partition simulated data into different subsets with distinct patterns. Then, the association rule mining (ARM) technique was applied to each dataset to extract

rules as recommendations for positive, negative, and neutral energy saving in favor of a selected façade panel. This framework provides simple recommendations on the energy performance of façade systems for different building types in different climate zones. The applicability of the proposed framework was tested on an innovative ultra-high-performance fiber-reinforced-concrete (UHP-FRC) façade panel. The extracted recommendations were validated using four different building models in different locations, which were not previously included in the building energy simulations. Results highlight the applicability of the proposed methodology in facilitating the energy performance analysis of different façade systems in different building contexts. This methodology can be used by designers as a decision support system to provide simple recommendations in the early stages of building envelope designs to obtain high-performance buildings.

6.1 Methodology

A data-driven framework is proposed to extract underlying structures and interactions from the thermal behavior of a façade system along with considering the combined effect of the building context and climate conditions to support decision-making. Figure 6-1 presents the proposed framework. The framework consists of two main steps: 1) BESs, which are conducted to create a database on the thermal behavior of the UHP-FRC façade system in a set of scenarios; and 2)

knowledge discovery and pattern recognition from the database using data mining techniques. In the first step, building models are simulated to estimate the energy performance of the UHP-FRC façade system for critical conditions so that the context in which the façade panel is being evaluated can represent all possible conditions. Then, underlying hidden structures are identified and extracted by exploiting the advantages of data mining techniques. These two main steps are further elaborated in the following sections.

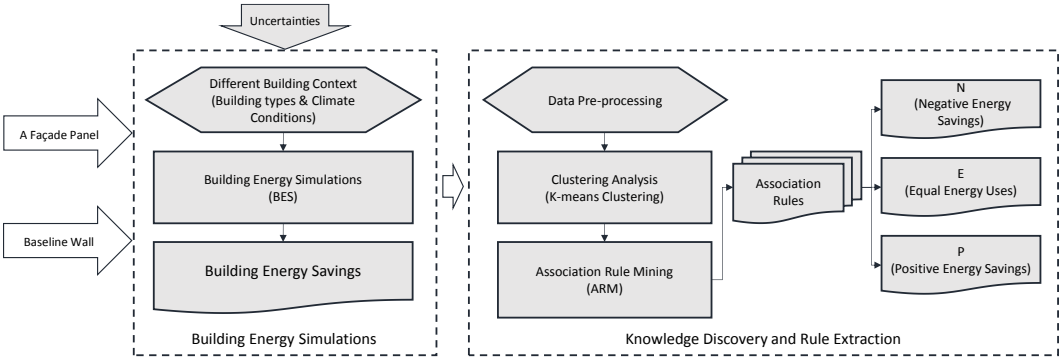

Figure 6-1 Proposed framework for knowledge discovery and rule extraction

6.1.1 Building Energy Simulations

In the first step, the thermal behavior of the UHP-FRC façade panel is explored in different building contexts and climate conditions under uncertainty. *EnergyPlus*™ (U.S. Department of Energy, 2018) is used to estimate the energy use of different building types in different weather conditions before and after

replacing the baseline façade panel with the UHP-FRC façade system to calculate the amount of energy savings. A conventional façade panel is selected as the baseline panel. Figure 6-2 shows the configuration of both UHP-FRC and conventional façade panels. The main difference between the conventional panel and the UHP-FRC panel is the type of concrete used for structural layers of the panels. Reinforced precast concrete is used for the exterior and interior wythes of the conventional panel. On the other hand, UHP-FRC concrete is used for the structural layers of the UHP-FRC panel. Higher cracking resistance provided by UHP-FRC concrete (three times greater than the cracking resistance of conventional concrete) allows designers to remove the reinforcing rebars from the structural layers of the panel and reduce the thickness of these structural layers. Therefore, more space is available for the insulation layer in the middle of the panel. Table 6-1 shows the thermal properties of panel layers for both UHP-FRC and conventional panels.

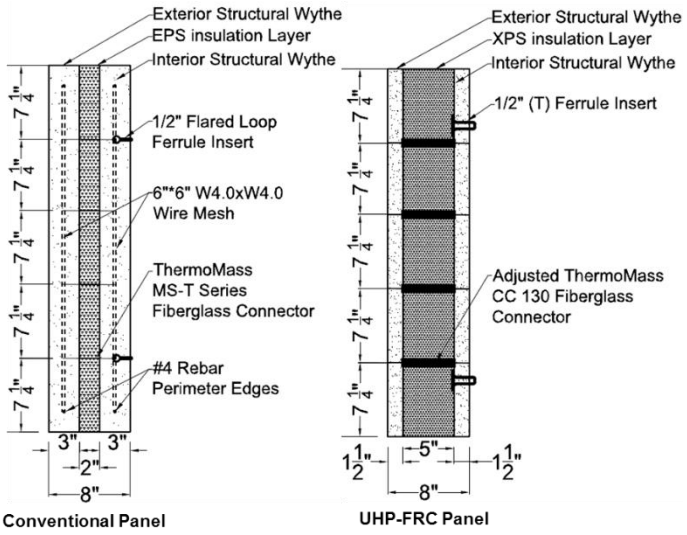

Figure 6-2 Conventional panel and UHP-FRC panel configuration

Table 6-1 Thermo-physical properties of UHP-FRC and conventional panels

Items	Parameters	Unit	Conventional Panel	UHP-RFC Panel
Concrete layer	Thickness (D)	cm	7.62 (3 in)	3.81 (1.5 in)
	Density (ρ)	kg/m3	2322	2403
	Porosity (P)	m3/m3	0.7912	0.7912
	Specific heat capacity (Cp)	J/kg-K	832	1010
	Thermal conductivity (λ)	W/m-K	2.31	1.77
	Vapor diffusion resistance (μ)	-	18.58	18.58
	Initial moisture content (MC)	kg/m3	19.22	20
Insulation layer	Thickness (D)	cm	5.08 (2 in)	12.7 (5 in)
	Density (ρ)	kg/m3	28	20
	Porosity (P)	m3/m3	0.99	0.99
	Specific heat capacity (Cp)	J/kg-K	645	645
	Thermal conductivity (λ)	W/m-K	0.005769	0.005769
	Vapor diffusion resistance (μ)	-	73.02	170.55
	Initial moisture content (MC)	kg/m3	0.06	0.13

6.1.2 Building Context

DOE commercial prototype buildings were used to represent the building context in this study. These prototype buildings characterize about 80% of the commercial building floor area in the U.S. for new construction, which include both commercial and mid- to high-rise residential buildings (Department of Energy, 2018). These building prototypes have been modeled based on the ANSI/ASHRAE/IES Standard 90.1 (Haverson et al., 2014). Fourteen DOE building models including high-rise and mid-rise apartments, a large hotel, small a hotel, a primary school, a secondary school, a fast food restaurant, a strip mall, a stand-alone retail store, a warehouse, a small office, a mid-size office, a large office, and a hospital were used as building models in this study. Figure 6-3 shows the 3D model of these prototype buildings. The exterior walls of these building models were replaced with the competing façade panels (conventional and UHP-FRC panels).

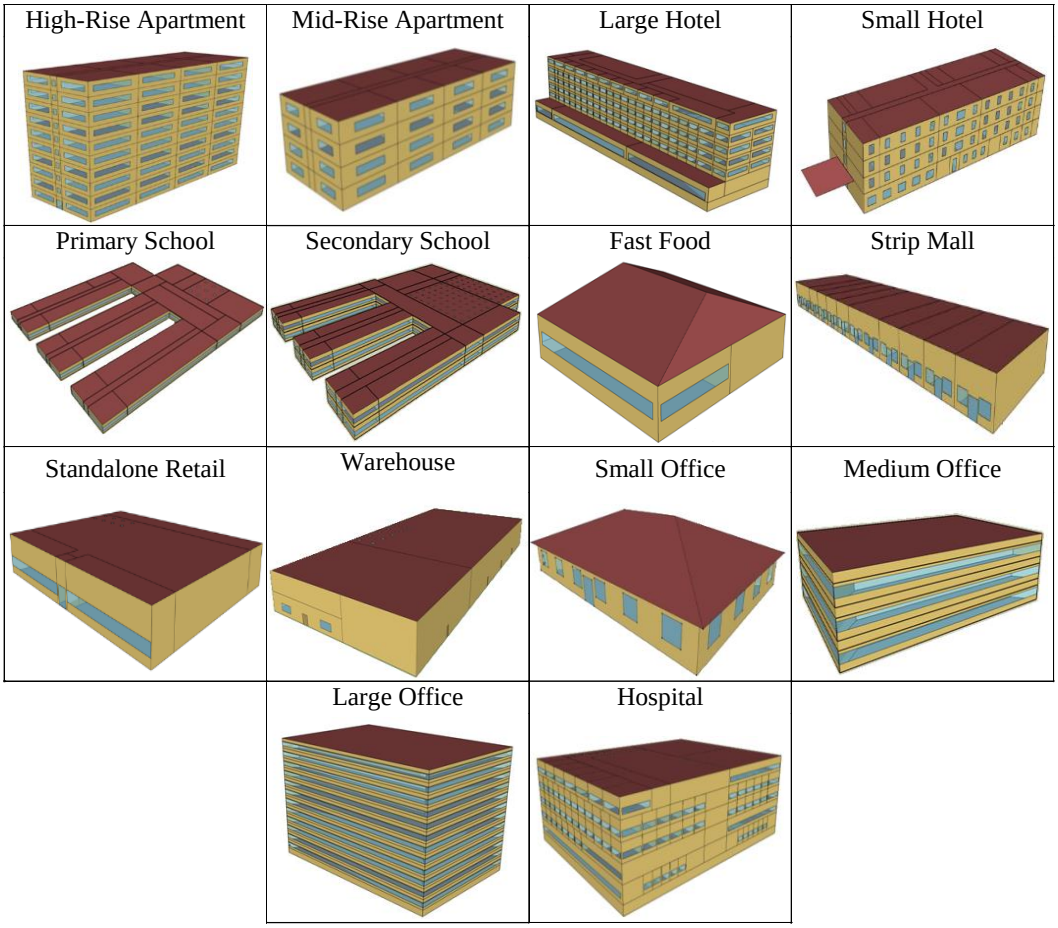

Figure 6-3 3D model of DOE prototype buildings

6.1.3 DOE climate zones and representative cities

DOE climate zones were used to represent different climate conditions in this study. These climate zones have been developed based on Solar and Meteorological Surface Observation Network (SAMSON) weather data (NREL, 1993). They provide consistent weather and climate conditions for all compliance methods and code sections of DOE and ASHRAE Standard 90.1–2004 (Briggs et

al., 2003). Fifteen typical locations (cities) were selected to represent all possible climate conditions in the U.S. Figure 6-4 illustrates the distribution of these cities across the U.S.

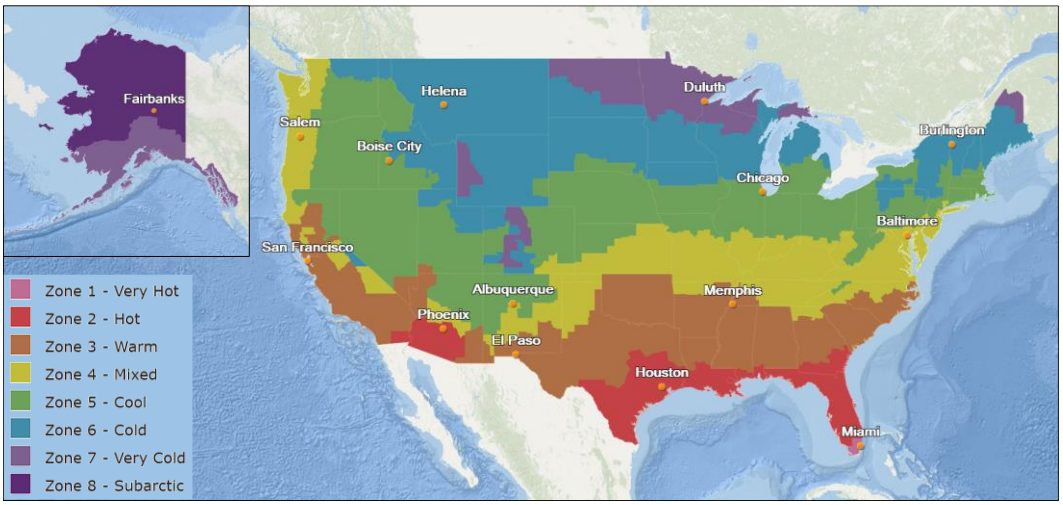

Figure 6-4 DOE climate zones and representative cities (U.S. Department of Energy, 2018)

6.1.4 Scenarios under uncertainty

Buildings as complex systems are characterized by multiple parameters including design geometry, material properties, occupancy, and system operations (Coakley et al., 2014). Various sources of uncertainty exist in buildings (Macdonald & Strachan, 2001; DeWit, S. & Augenbroe, 2002) that can result in a major discrepancy between the simulated and actual energy use of buildings (Coakley et al., 2014). In this study, major sources of uncertainty in design input parameters were considered in the building energy simulations to reduce the amount of

discrepancy between the simulated and actual energy use of buildings. Three critical input parameters—infiltration rate, occupancy level, and lighting loads, which are highly recommended by researchers (Hopfe et al., 2007; Li et al., 2015; Soto et al., 2015; Berkeley et al., 2015; and Menberg et al., 2016), were considered as the uncertain parameters in the simulations. In addition, six thermo-physical properties of façade panels were included. Recommended probability distributions, mean values, and standard deviations of each uncertain parameter were extracted from the literature to generate random values for each parameter. A hundred iterations were randomly sampled using the Latin hypercube sampling (LHS) method (Mckay et al., 2000) for each building model to create pools of randomly generated models for each scenario. Monte Carlo methods have been used by several researchers in different engineering fields, such as building energy simulations (Asadi et al., 2014) and water pipe networks rehabilitation (Pudasaini et al., 2017; Pudasaini and Shahandashti, 2018; Shahandashti and Pudasaini, 2019). The sampled building models were simulated using *EnergyPlus* to estimate the energy consumption of buildings enhanced with the UHP-FRC panels and to compare them with the energy consumption of buildings with the conventional panels in the context of 14 building types in 15 different locations (210 scenarios). In total, 21000 simulations were conducted for both buildings with the conventional panels and buildings with the UHP-FRC panels, and the energy savings were calculated in favor of UHP-RC panels. A positive value of energy savings indicates

that replacing the baseline panel with the UHP-FRC panel will result in positive building energy savings for the given conditions.

6.1.5 Building Energy Simulated Data

The results of BESs were used to create a database to feed the second part of the framework, which is knowledge discovery. The simulated data includes information about the amount of energy savings for different buildings enhanced with the UHP-FRC façade panel in different locations. The corresponding properties of each building and location were derived into attributes to create the database. For example, each DOE prototype building is represented by several parameters including building heating and cooling systems, total floor area, number of floors, building aspect ratio, and window fraction. Each location's climate condition was also derived by the most important weather parameters recommended by researchers Neto & Fiorelli (2008) and Zhao & Magoulès (2012). Therefore, the database consists of 21000 data points with 44 explanatory variables including building design parameters (seven variables), weather-related parameters (28 variables), and building uncertain parameters (nine variables), and five target variables including the amount of energy savings. This database covers most of the possible combinations of weather conditions and building types in the U.S.

6.2 Knowledge Discovery

The purpose of this section is to present the methodology used to extract underlying and hidden structures from the energy savings of buildings using data mining techniques. First, the simulated data is pre-processed to enhance the quality of the data. Different statistical techniques are used to investigate the correlations between the variables and measure explanatory variables' contribution to the target values. Then, the clustering analysis is applied to discover underlying patterns in the data by partitioning it into different datasets with higher internal similarities. In the end, association rule mining (ARM) is used to extract rules from each dataset.

6.2.1 Data Preprocessing

Data preprocessing helps to enhance the quality of data by removing outliers and inconsistencies (Lai & Leu, 2016). Data outliers can result in dramatic changes in the performance of the outputs of an energy performance model (Lu et al., 2014; Ashuri et al., 2019). Since the data used for this study is simulated data, the dataset does not include missing values or outliers. Spearman's rank-order correlation was used to investigate the correlations between the variables since the variables do not follow the normal distribution. The data includes different attributes with different measurement units. For example, the unit of heating energy usage is gigajoule (GJ), but the building total floor area unit is a square meter (m^2). Therefore, the minimum

and maximum (min-max) data normalization technique was applied to the numerical parameters to reduce the effect of measurement units on the results and to speed up the algorithm computation. Equation 6-1 illustrates the min-max normalization for heating energy use as an example:

$$THEU' = \frac{HEU - HEU_{min}}{HEU_{max} - HEU_{min}} \quad \text{Equation 6-1}$$

where *HEU'* is the normalized heating energy use, *HEU* is the original value of heating energy use, and HEU_{min} and HEU_{max} represent the minimum and maximum values of heating energy use.

6.2.2 Clustering

Clustering analysis is a data mining technique that partitions a dataset into a number of clusters that are internally coherent and externally separated. In other words, it aims to maximize the similarities between data points in the same cluster while minimizing similarities between clusters (Abonyi & Feil, 2007). In clustering analysis, each data point is treated as an object, which is located in an n-dimensional feature space. The location of each data point is determined by calculating a distance metric (proximity measure), which defines the similarities and dissimilarities between the data points (Kotsiantis & Pintelas, 2004.). Clustering algorithms, such as hierarchical clustering (connectivity-based clustering),

centroid-based clustering (k-means), and distribution and density-based clustering, are capable of dividing multidimensional and heterogeneous data space into sub-regions with similarities in that the center of each cluster can be used for representing a typical pattern within data features (Orlandic et al., 2005).

The *K*-means clustering algorithm is one of the most popular clustering techniques among researchers in various fields since it is a robust technique in identifying clusters (Wagstaff et al., 2001). K-means clustering was used to cluster the simulated data into several clusters due to its robustness and ease of implementation. K-means divides data points into k exclusive clusters with the nearest centroid or mean (Gao & Malkawi, 2014). Each data point is represented by a vector in an n-dimensional feature space. Centroids are representatives of the corresponding clusters. The objective function for the *K*-means algorithm puts each data point into a cluster to minimize dissimilarity between the data point and the centroid of the cluster (Eq. 6-2).

$$Obj = \sum_{j=1}^{k} \sum_{i=1}^{n} \min_{\mu_j} \left\| x_i - \mu_j \right\| \qquad \text{Equation 6-2}$$

where x_i is the i^{th} vector representing a data point in a specific condition, μ_j is the mean (centroid) of all the vectors belonging to the j^{th} cluster, n is the number of vectors (e.g., 21000), and $||x_i-\mu_j||$ indicates the Euclidean distance between each data point and the centroid of the corresponding cluster. The K-mean algorithm

iteratively assigns each data point to one of the *k* clusters based on those provided. The algorithm starts the first iteration with random initialization centroids (*k*) and assigns each data point to each centroid to minimize the objective function. In the next iteration, new centroids are calculated for the clusters, and the data points are reassigned to the new centroids. This process is repeated until the cluster membership stabilizes and the algorithm is converged (Jain and Dubes, 1988).

K-means requires specifying the *k* number, which can be quite difficult if prior knowledge is limited. Clustering performance metrics such as the silhouette and Davies-Bouldin indexes were used to identify the optimum *k* number for the clustering analysis. These indexes test the performance of clustering analysis for given cluster numbers. They test whether the clustering results satisfy the assumption that members of a cluster are more similar than members of other clusters based on similarity metrics (Nikolaou et al., 2012).

6.2.3 Association Rule Mining

After partitioning the dataset into different clusters with similar characteristics, ARM was used to extract associations within the attributes of each cluster and express extracted knowledge in a rule format. ARM is a powerful data mining tool that can help researchers understand and interpret complicated associations and interactions in a dataset (Han & Kamber, 2012). ARM has been

successfully applied in various research communities such as marketing and business; furthermore, its applications are emerging in building research communities as well (Cabrera & Zareipour, 2013; Xiao & Fan, 2014; Rollins & Banerjee, 2014).

An association rule can be defined as $X \rightarrow Y$. X is called antecedent, and Y is called consequent. Therefore, $X \rightarrow Y$ means that if X happens, then Y will happen. For example, assume that a rule is defined as "total floor area (*TFA*) → cooling energy savings (*CES*)". This means that if *TFA* increases, then *CES* will also increase. Support and confidence are the two main parameters in ARM. Support is the joint probability of X and Y (i.e., $P(X \text{ and } Y)$). Higher support tends to find rules that happen frequently. The other parameter, confidence, is defined as a conditional probability of Y given X (i.e., $P(Y|X)$). Higher confidence ensures that the association rules are well supported by data and more important (Han & Kamber, 2012). The number of association rules extracted by ARM depends on the threshold of both support and confidence. A larger threshold for support results in discovering a higher number of association rules. On the other hand, setting a higher threshold for confidence (usually more than 80 percent) ensures the extraction of useful association rules. Lift is another parameter that is commonly used for selecting useful association rules. It is defined as the ratio of confidence ($X \rightarrow Y$) to support (Y). A lift value higher than 1 indicates that the occurrence of X positively affects the occurrence of Y. Adversely, a lift value lower than 1 means that the occurrence

of *X* negatively affects the occurrence of *Y*. Both conditions indicate that the occurrence of *Y* is dependent on the occurrence of *X*. If the lift index is equal to 1, it means that the occurrences of *X* and *Y* are independent, so the association rule is meaningless.

Conventional ARM algorithms, such as Apriori and Frequent-pattern growth (Ft-growth), are two popular algorithms for association rule mining (Pramudiono & Kitsuregawa, 2003; Al-Maolegi & Arkok, 2014). However, they are only able to extract association rules from categorical antecedents and consequents. Therefore, numerical data is required to convert to categorical data that may reduce the quality of extracted rules. On the other hand, a quantitative ARM (QARM) algorithm can extract rules from both categorical and numerical variables (Adhikary & Roy, 2015). For the same example, a rule pattern is defined as $TFA \rightarrow CES$ in QARM, where *TFA* and *CES* are continuous variables (i.e., $TFA \in [a_1, a_2]$ and $CES \in [b_1, b_2]$), and a_1, a_2, b_1, and b_2 are the intervals for *TFA* and *CES*.

In this study, QARM (see Salleb-Aouissi et al., 2007 and Salleb-Aouissi et al., 2013) was used to extract association rules from the clusters. Since the energy savings for heating, cooling, total heating and cooling, and total site energy savings were numeric variables, they were coded into groups: *N* (negative energy savings), *E* (no energy savings), and *P* (positive energy savings). A rule with conclusion *N*

indicates that the energy savings is negative when the conventional panel is replaced with the UHP-FRC panel in given conditions. On the other hand, a rule with *P* shows that replacing the conventional panel with a UHP-FRC panel will result in positive energy savings in the given conditions, and finally, a rule with *E* states that there is no difference between two panels in terms of building energy savings in the given conditions.

6.2 Results and Discussion

6.2.1 Descriptive Statistics

Figure 6-5 illustrates the frequency distribution of the important explanatory variables. This figure shows that none of the variables follows a normal distribution. Table 6-2 shows the Spearman rank correlations between the explanatory variables. As it was expected, weather-related variables are highly correlated. Strong correlations also exist between some of building physical variables, such as total floor area, number of floors. Table 6-3 shows the Spearman rank correlations between the explanatory and target variables. Window fraction and number of floors are two variables with high positive correlations with the target variables. On the other hand, aspect ratio, total floor area, wind speed, lighting, and occupancy level have small correlation coefficients with the target variables. A high correlation was expected between the total floor area and the building energy uses since increasing the total floor area would increase the

building conditioned area. However, the result shows a weak correlation between the total floor area and all building energy uses.

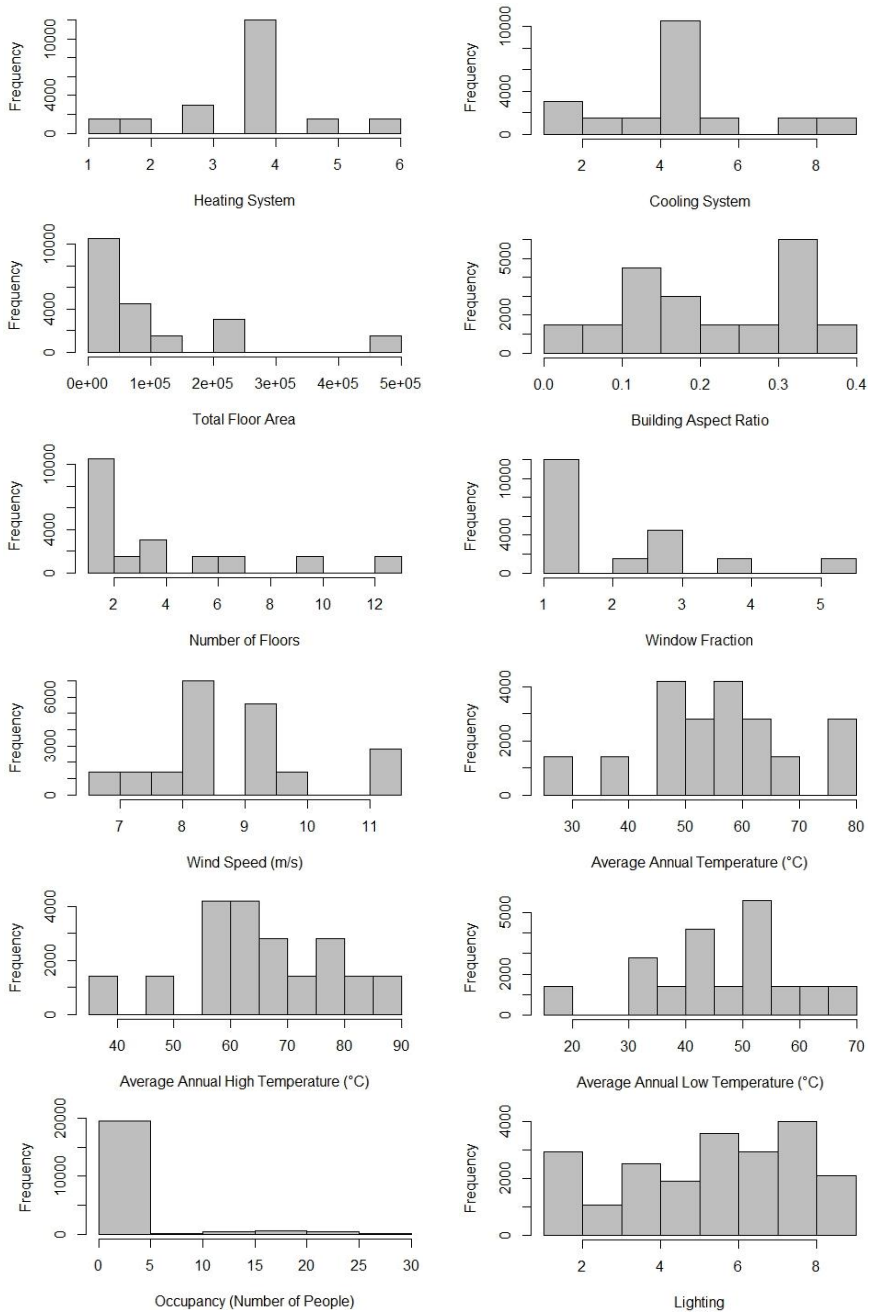

Figure 6-5 Frequency distribution of input variables

Table 6-2 Spearman rank correlation between input variables

	TFA	AR	NF	WF	AAHT	AALT	AAT	WS	L	OL
Total Floor Area	1	0.605	0.719	0.073	0	0	0	0	0	0.199
Aspect Ratio	0.605	1	0.461	-0.082	0	0	0	0	0	0.199
Number of Floors	0.719	0.461	1	0.405	0	0	0	0	0	0.208
Window Fraction	0.073	-0.082	0.405	1	0	0	0	0	0	-0.015
Average Annual High Temperature	0	0	0	0	1	0.971	0.979	-0.174	0	0
Average Annual Low Temperature	0	0	0	0	0.971	1	0.993	-0.197	0	0
Average Annual Temperature	0	0	0	0	0.979	0.993	1	-0.191	0	0
Wind Speed	0	0	0	0	-0.174	-0.197	-0.191	1	0	0
Lighting	0	0	0	0	0	0	0	0	1	-0.076
Occupancy Level	0.199	0.199	0.208	-0.015	0	0	0	0	-0.076	1

Table 6-3 Spearman rank correlation between input and output variables

	Total Site Energy Use	Total Heating Energy Use	Heating Energy Use (Electricity)	Heating Energy Use (Gas)	Cooling Energy Use (Electricity)
Total Floor Area	0.063	0.075	-0.037	0.081	-0.014
Aspect Ratio	0.008	0.024	0.043	-0.007	0.048
Number of Floors	0.228	0.206	0.191	0.171	0.145
Window Fraction	0.392	0.276	0.246	0.227	0.269
Average Annual High Temperature	-0.317	-0.587	-0.207	-0.560	0.382
Average Annual Low Temperature	-0.335	-0.593	-0.211	-0.567	0.334
Average Annual Temperature	-0.324	-0.588	-0.212	-0.562	0.354
Wind Speed	-0.094	0.037	0.031	0.036	-0.198
Lighting	-0.043	-0.027	-0.023	-0.019	-0.056
Occupancy Level	-0.057	-0.042	-0.005	-0.044	-0.018

6.2.2 Results of Clustering Analysis

Silhouette and Davies-Bouldin indexes were used to find the optimum number of k for the clustering analysis. A higher silhouette index and lower Davies-Bouldin index guaranteed consistency within the clusters. Figure 6-6 illustrates the silhouette and Davies-Bouldin values for different k numbers (2 to 10). Both indexes show that the K-means clustering algorithm performs better when the number of clusters is set to four. Therefore, the K-means clustering technique was used to partition the simulated building energy data into four clusters.

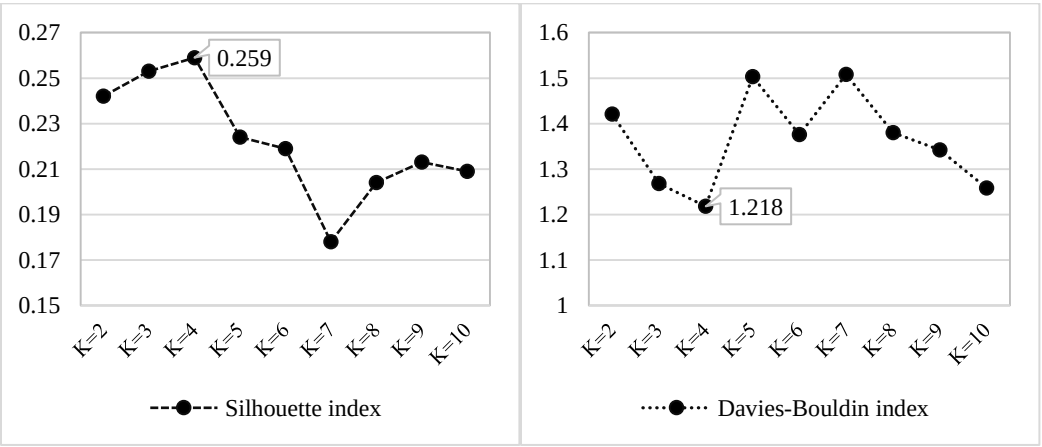

Figure 6-6 Clustering validation results with silhouette and Davies-Bouldin indexes

The principal component analysis (PCA) was used to represent the multi-dimensional data points in a two-dimensional feature space through two principal components (Figure 6-7). PCAs are orthogonal components that explain the

variation in the original data. The PCA result shows that Cluster 1 and Cluster 2 have lower variation compared to the other two clusters.

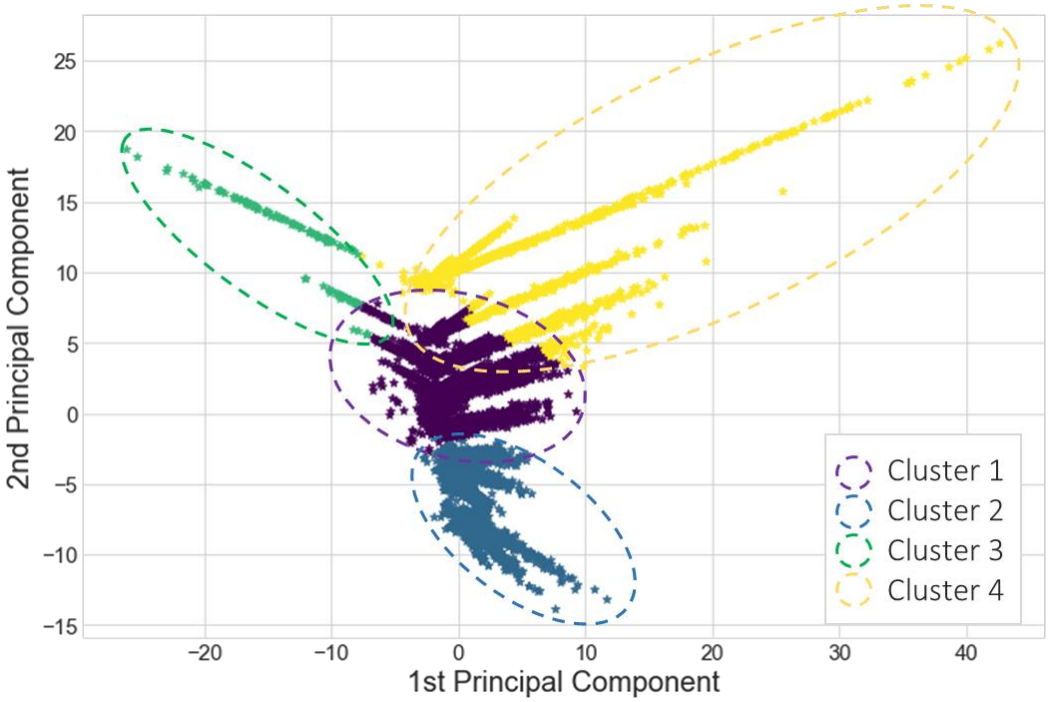

Figure 6-7 Representation of data points within four clusters in a two-dimensional feature space using two principal components

Table 6-4 shows the mean values for the key parameters in each cluster. Cluster 1 and Cluster 3 were the largest and smallest clusters with 11979 (about 57%) and 140 (less than 1%) data points, respectively. Comparing parameter centers for the clusters shows that Cluster 1 mainly represents all types of buildings located in temperate locations. Also, Cluster 2 represents all types of buildings located in warmer locations with higher annual high and low temperatures. Buildings in Cluster 2 have the lowest amount of energy savings for all the energy

saving categories compared to the other clusters. Cluster 3 only represents the mid-size office building located in very cold locations such as Fairbanks and Burlington. In this cluster, although the UHP-FRC façade panel has the worst performance of keeping cooling energy use down but performs very well at maintaining heating energy use costs at an acceptable level. Finally, Cluster 4 mostly represents buildings located in Sub-Arctic and very cold locations such as Fairbanks and Duluth. This cluster has the highest amount of energy savings for cooling and heating and site energy uses.

Table 6-4 Attribute centroids and the number of instances within each cluster

Parameters		All Data		Cluster							
				1		2		3		4	
		STD	ORIG	STD	ORIG	STD	ORIG	STD	ORIG	STD	ORIG
Building physical parameters	TFA	0.296	9732	0.221	9583	0.302	9841	0.165	4979	0.484	11322
	AR	0.537	0.2	0.516	0.2	0.547	0.2	0.928	0.3	0.632	0.2
	NF	0.339	3.9	0.242	3.8	0.326	3.9	0.333	3.0	0.376	4.1
	WF	0.286	2.2	0.175	1.9	0.271	2.2	0.058	1.5	0.360	2.5
Weather-related parameters	AHT	0.558	65.6	0.476	61.1	0.848	79.7	0.076	41.6	0.097	42.6
	ALT	0.538	45.8	0.460	41.4	0.798	59.6	0.083	21.6	0.095	22.2
	AAT	0.564	55.7	0.479	51.3	0.843	69.6	0.082	31.6	0.099	32.4
	WS	0.484	10.2	0.626	10.9	0.333	9.4	0.212	8.8	0.194	8.7
Energy savings	CES	0.154	10.9	0.133	8.1	0.190	3.9	0.120	34.5	0.116	46.4
	HES	0.146	9.0	0.119	7.1	0.104	0.5	0.201	34.3	0.329	44.1
	THCES	0.158	1.0	0.124	0.4	0.125	2.2	0.205	0.2	0.330	0.3
	TSES	0.166	10.1	0.132	7.5	0.136	2.8	0.208	34.5	0.336	44.4
Number of instances		21000		11979		6996		140		1884	
%		100.00%		57.00%		33.00%		0.70%		9.00%	

Overall, the results of clustering analysis show that the k-means algorithm mostly partitioned the dataset into clusters based on weather-related parameters. Even in Cluster 3, which only includes medium office buildings, the office buildings located in very cold locations were separated from other buildings by the clustering algorithm.

6.2.3 Results of Association Rule Mining

Quantitative association rule mining was applied to the clusters to extract associations among the attributes of each cluster. We set the categorical energy savings (heating, cooling, total heating and cooling, and total site energy savings) as consequents, and building and weather-related parameters as antecedents. The threshold for support and confidence was 40% and 90%, respectively. The lift index was used to sort the rules based on their level of interest. The lift threshold was set at 1.20 to select the more important positive correlations among the attributes of each cluster. In total, 13 rules were extracted from four clusters as the most important rules. Table 6-5 illustrates the selected rules for three clusters.

Table 6-5 Extracted association rules from Cluster 1, 2, and 4

Cluster	Rule			Support	Confidence	Lift
	Premise		Conclusion			
Cluster 1 (11979 records)	HS & WS	[Gas-fired Boiler] & [9.3; 11.1]	TSEU & THCEU (P)	40.48%	92.45%	1.2
	TFA	[3130 - 11346]	TSEU & THCEU (P)	44.95%	90.90%	1.2
Cluster 2 (6996 Records)	TFA	[232- 4013]	TSEU & THCEU & CEU (P)	40.29%	93.10%	1.2
	TFA & ALT	[232 - 4013] & [51.8 - 69.9]	TSEU & CEU (P)	40.29%	93.10%	1.2
	TFA & AAT	[232 - 4013] & [63.0 - 77.05]	TSEU & CEU (P)	40.29%	93.10%	1.2
	NF	[1 - 4]	TSEU & THCEU & CEU (P)	40.29%	93.10%	1.2
	WF	[1 - 4]	TSEU & THCEU & CEU (P)	40.29%	93.10%	1.2
	AHT	[72.4 - 86.7]	TSEU (P)	40.61%	94.73%	1.2
	ALT	[51.8 - 69.9]	TSEU (P)	40.61%	94.73%	1.2
	AAT	[63.0 - 77.05]	TSEU (P)	40.29%	93.10%	1.2
Cluster 4 (1884 Records)	TFA	[11346- 19593]	TSEU & THCEU & CEU (P)	42.97%	96.14%	1.3
	WS	[7.7 - 11.0]	THCEU & CEU (P)	42.97%	96.14%	1.3
	WS & TFA	[7.7 - 11.0] & [11346- 19593]	CEU (P)	42.97%	96.14%	1.3

Investigating the rules by considering each cluster's properties shows that the rules are reasonable and logical. It is observed that no rule has been extracted from Cluster 3 since the dataset only represents medium office buildings in cold locations with 140 data points. Like the clustering analysis, which distinguished the energy performance of a medium office building enhanced with UHP-FRC panels as a distinct pattern, ARM also found a specific energy performance pattern for the mid-size office building in cold locations with no rule. Therefore, it is safe to state that replacing conventional panels with UHP-FRC panels in a building like the medium office building in locations with cold weather conditions results in positive building energy savings. Cluster 1, the largest cluster with the fewest variations (Figure 6-7), mostly represents buildings in temperate locations with a low rate of

energy savings. Only two important rules with a lift index higher than 1.20 have been extracted from Cluster 1. These two rules are mostly related to the physical properties of buildings. The first rule states that in locations with relatively lower wind speeds (the wind speed range for this cluster was [9.3–12.8 m/s]), using a gas-fired boiler heating system will more likely result in positive total site energy and total heating and cooling energy savings. The second rule indicates that buildings with a relatively lower floor area [3130–11346 m^2] will more likely have positive savings in the total site, total heating, and cooling energy uses.

Eight association rules were extracted from Cluster 2. Like Cluster 1, Cluster 2 has a higher number of data points. However, the variations in Cluster 2 is relatively higher compared to Cluster 1 (Figure 6-7). This is the reason that a higher number of rules were extracted from this cluster. The total floor area was the most frequent parameter displayed in the rules as the antecedent. The number of floors, window fraction, and the annual high and low temperatures were the other parameters displayed in the extracted rules. Buildings with the relatively lower floor area, low number of floors, and lower window fraction located in places with higher annual high and low temperatures were more likely to have positive cooling and heating energy savings. Three association rules were also extracted from Cluster 4. These rules include wind speed and total floor area as antecedents. Buildings with a relatively higher total floor area in the locations with relatively

lower wind speed are more likely to have positive savings in cooling and heating energy uses.

Investigating the results of clustering analysis and QARM together shows that clustering analysis mostly partitioned the dataset into clusters based on weather-related parameters. For example, the clustering algorithm identified Cluster 1 as buildings mostly located in temperate weather conditions, while Cluster 2 included the buildings located in the cold locations. On the other hand, ARM extracted rules from the clusters mostly based on the physical properties of buildings, such as heating system, total floor area, number of floors, and window fraction, incorporated with some weather-related parameters. It is also interesting that the correlation results showed no strong correlation between the total floor area and the energy savings. However, the proposed framework could extract a rule for each cluster related to the total floor area. This shows the importance of data mining techniques in the extraction of hidden patterns, underlying structures, and nonlinear interactions from the data, which would not be possible using common statistical approaches, such as correlation analysis.

6.3 Validation

Four different building models, which were not previously used in the simulations and database, were used to validate the extracted association rules

(Figure 8). Table 6-6 shows a detailed description of building models and their locations. According to the models' physical properties and locations, the hotel, strip mall, office, and apartment can be classified into Cluster 1, 2, 3, and 4, respectively. Based on the extracted rules for each cluster, it is expected that all building energy savings be positive for all building models, except for the cooling energy use of the office building. Table 6-7 shows the simulated energy savings of all four buildings by EnergyPlus^{TM}. The results show that all the energy savings are consistent with the extracted rules.

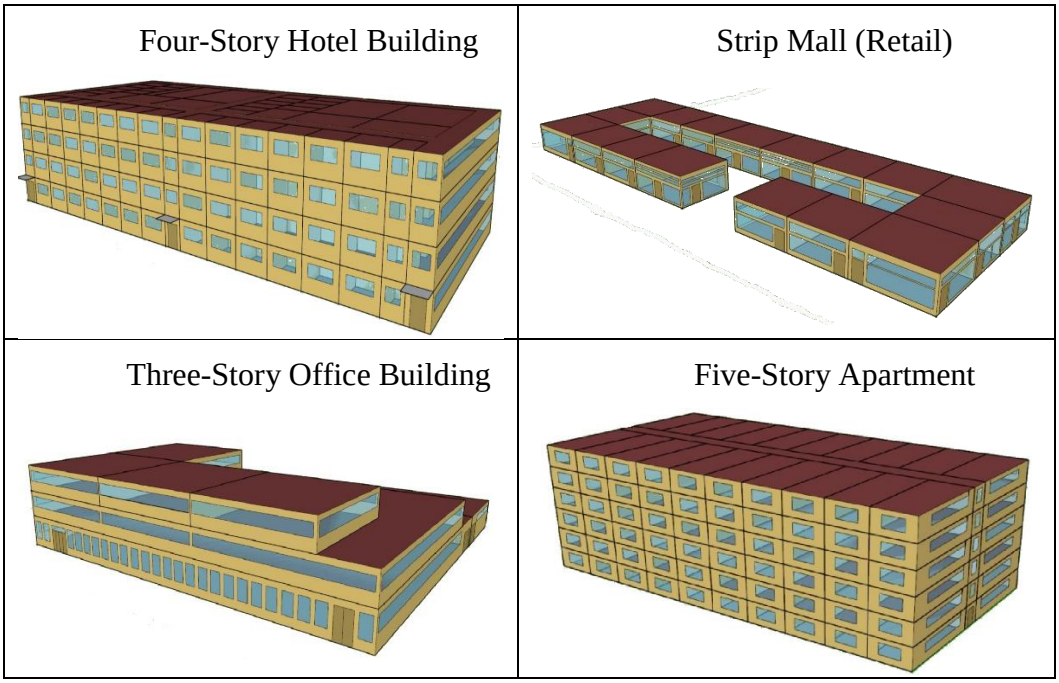

Figure 6-8 3D model of buildings used for validation

Table 6-6 Description of selected buildings for validation

ID	Building type	Total floor Area*	Window Fraction	Number of Floors	Aspect ratio	Cooling system	Heating system	Location
1	Mid-size Hotel	10050	0.1	4	2.2	Centrifugal Chillers	Gas-fired Boiler	Knoxville, IA
2	Strip Mall (Retail)	1064	0.52	1	-	PTAC, Split system	PTAC, Split system	Corpus Christi, TX
3	Office Building	5035	0.36	3	-	PTAC, Split system	PTAC, Split system	Bethel, AK
4	Mid-rise Apartment	11613	0.1	6	2	Split system DX	Gas furnace	Anchorage, AK

*square meters

Table 6-7 Building energy savings

ID	Building type	Location	Energy savings (GJ)			
			Total site energy use	Total heating and cooling	Heating	Cooling
1	Mid-size Hotel	Knoxville, IA	159.35	158.81	150.80	8.01
2	Strip Mall (Retail)	Corpus Christi, TX	2.00	1.97	1.49	0.48
3	Office Building	Bethel, AK	7.68	11.82	9.77	-2.05
4	Mid-rise Apartment	Anchorage, AK	80.34	79.00	78.80	0.20

CHAPTER 7

CONCLUSIONS AND FUTURE WORK

7.1 Conclusions

The energy performance of the innovative UHP-FRC façade panel was evaluated in both assembly-scale and building context. In assembly scale, the hygrothermal performance of UHP-FRC panel was investigated using heat and moisture transfer for different ambient conditions. The results of hygrothermal assessment showed that the implementation of the UHP-FRC panel could decrease the risk of condensation and mold growth behind the insulation layer in comparison with the conventional panel. In addition to the hygrothermal assessment within the UHP-FRC panel, the effect of steel connections proposed by Precast/Prestressed Concrete Institute (PCI) in the hygrothermal performance of UHP-FRC panel was also investigated. The results of heat transfer analysis showed that steel connections could significantly reduce the thermal resistivity of façade panels by converging heat fluxes and acting as thermal bridges within façade panels. The results also showed that the maximum heat flux in the steel connector of the panel to foundation connection had ten times higher compared to the other connections. In addition, the results of moisture transfer showed that air gaps between the panels had higher moisture flux magnitude compared to the other layers in the connections. However,

the risk of mold growth was very low due to very low level of moisture content within the panel.

In the building context, the building energy performance of UHP-FRC was evaluated for different locations and different building types (210 scenarios) using building energy simulations. The results of building energy simulations and hypothesis tests showed that buildings with UHP-FRC façade panels consume less energy than the buildings with conventional panels in most of the scenarios (133 scenarios out of 210). In the 76 scenarios, the buildings with UHP-FRC façade panels perform similarly to the buildings with conventional panels. Only in one scenario (warehouse in El Paso), the buildings with the conventional panels outperform the buildings with the UHP-FRC façade panels. Although UHP-FRC façade systems have thicker insulation layers with higher R-value compared with the conventional panels, they do not necessarily result in building energy reduction; the energy savings of using UHP-FRC panels depend on the building type and climate condition. The energy performance assessment of innovative façade systems such as UHP-FRC panels could be misleading if the diversity of building types and climate contexts are not taken into account. On average, savings are higher in colder climates (e.g., Fairbanks) than those in temperate climates (e.g., San Francisco). Also, on average, buildings that are dominated by internal loads (e.g., fast food restaurants where all energy savings are within 1 percent) seem to benefit the least from UHP-FRC. Since the building energy simulations were

conducted for a set of scenarios, a data-driven framework was also developed to extract hidden information and underlying structure from the thermal behavior of façade systems from the simulated data to provide recommendations to help designers to select energy-efficient façade systems. The results highlight the applicability of the proposed methodology in facilitating the energy performance analysis of UHP-FRC panels in different building contexts.

The benefits of this study go beyond just an investigating of the energy performance analysis of UHP-FRC façade panel, it equips building engineers with methodologies that can comprehensively investigate the energy performance of façade panels. It is expected that these methodologies provide building engineers with essential means to objectively appraise the energy performance of innovative façade systems in both assembly-scale and building context.

7.2 Future Work

There are some ideas that I would have liked to try. The following ideas could be tested:

- This framework is intended to provide recommendations for selecting a specific façade panel over a baseline façade panel in different conditions. Future studies should focus on adapting this framework to consider energy benchmarks of building energy

efficiency standards, such as the American Society of Heating, Refrigerating and Air-Conditioning Engineers (ASHRAE) and the International Energy Conservation Code (IECC), as baselines or integrating it with building energy benchmarking models, such as Data Envelopment Analysis (DEA).

- K-means algorithm, which is used for partitioning the database into clusters, is an iterative algorithm that its performance depends on the initial cluster centers (Gao and Malkawi, 2014). It means that final clustering results can be different with different initial cluster centers. Therefore, additional studies are required to investigate the effect of different clustering techniques, such as density-based spatial clustering of applications with noise (DBSCAN), expectation–maximization (EM) clustering, and agglomerative hierarchical clustering, on the extracted rules.
- It could be interesting to evaluate the framework on different façade systems with innovative materials, such as bioconcrete (Soleimani and Shahandashti, 2017) and phase change materials (Noël et al., 2016).
- The investment valuation of these innovative façade systems under uncertainty is recommended (Kashani et al., 2014; Kashani et al., 2012).

REFERENCES

Abdou, O. A., Murali, K., & Morsi, A. (1996). Thermal performance evaluation of a prefabricated fiber-reinforced plastic building envelope system. *Energy and buildings*, *24*(1), 77-83.

Abediniangerabi, B., Shahandashti, S. M., Bell, B., Chao, S. H., & Makhmalbaf, A. (2019). Assembly-Scale and Whole-Building Energy Performance Analysis of Ultra-High-Performance Fiber-Reinforced Concrete (UHP-FRC) Façade Systems.

Abediniangerabi, B., Shahandashti, S. M., Bell, B., Chao, S. H., & Makhmalbaf, A. (2018). Building energy performance analysis of ultra-high-performance fiber-reinforced concrete (UHP-FRC) façade systems. *Energy and Buildings*, *174*, 262-275.

Abonyi, J., & Feil, B. (2007). *Cluster analysis for data mining and system identification*. Springer Science & Business Media.

Adhikary, D., & Roy, S. (2015, July). Trends in quantitative association rule mining techniques. In *Recent Trends in Information Systems (ReTIS), 2015 IEEE 2nd International Conference on* (pp. 126-131). IEEE.

Aghdasi, P., Heid A. E., and Chao, S.-H. (2016), Developing Ultra-High-Performance Fiber-Reinforced Concrete For Large-Scale Structural

Applications, ACI Materials Journal, V. 113, No. 5, September-October 2016, pp. 559-570.

Ahlborn, T., Harris, D., Misson, D., and Peuse, E. (2011). Characterization of Strength and Durability of Ultra-High-Performance Concrete Under Variable Curing Conditions, Transportation Research Record: Journal of the Transportation Research Board, No. 2251, Transportation Research Board of the National Academies, Washington, D.C., 2011, pp. 68–75.

Al-Maolegi, M., & Arkok, B. (2014). An improved apriori algorithm for association rules. *arXiv preprint arXiv:1403.3948*.

Asadi, S., Amiri, S. S., & Mottahedi, M. (2014). On the development of multi-linear regression analysis to assess energy consumption in the early stages of building design. *Energy and Buildings*, *85*, 246-255.

Ashuri, B., Wang, J., Shahandashti, M., & Baek, M. (2019). A data envelopment analysis (DEA) model for building energy benchmarking. *Journal of Engineering, Design and Technology*.

Balocco, C., & Petrone, G. (2018). Mathematical Modelling of Engineering Problems. *Journal homepage: http://iieta. org/Journals/MMEP*, *5*(3), 146-152.

Bell, B., Shihabeddin, L., Essari, J., Arevalo, H., & Richardson, S. (2016). High Performance Precast Façade Panels, White paper, Link:

https://static1.squarespace.com/static/5588241ce4b0562ee8fe469a/t/57a74cd7b3db2b8908f4f2ef/1470581979516/UHPC+Panel_Final+Boards_11x17+%281%29.pdf, Last Visited: 12/12/2016.

Berkeley, P., Haves, P., & Kolderup, E. (2015). The Effect of Modeler Decisions on Simulation Uncertainty : Some Implications for User Interface Design. *Building Simulation 2015*: 14th Conference of International Building Performance Simulation Association (pp. 2923-2930). Hyderabad, India.

Bhamornsiri, C., Gomez, P., Wilson, T., & Eisenhower, B. (2013). Calibration of envelope parameters using control-based heat balance identification and uncertainty analysis. In *Proceedings of BS2013: 13th conference of international building performance simulation association. Chambéry (France)*.

Bhandari, M., Shrestha, S., & New, J. (2012). Evaluation of weather datasets for building energy simulation. *Energy and Buildings*, *49*, 109-118.

Briggs, R. S., Lucas, R. G., & Taylor, Z. T. (2003). Climate classification for building energy codes and standards: Part 2-Zone definitions, maps, and comparisons. *Transactions-American Society of Heating Refrigerating and Air Conditioning Engineers*, *109*(1), 122-130.

Cabrera, D. F. M., & Zareipour, H. (2013). Data association mining for identifying lighting energy waste patterns in educational institutes. *Energy and Buildings*, *62*, 210-216.

Chan, A. L. S., Chow, T. T., Fong, K. F., & Lin, Z. (2009). Investigation on energy performance of double skin facade in Hong Kong. *Energy and Buildings*, *41*(11), 1135-1142.

Chang, W. J., & Weng, C. I. (2000). An analytical solution to coupled heat and moisture diffusion transfer in porous materials. *international Journal of heat and mass transfer*, *43*(19), 3621-3632.

Cheung, C. K., Fuller, R. J., & Luther, M. B. (2005). Energy-efficient envelope design for high-rise apartments. *Energy and buildings*, *37*(1), 37-48.

Coakley, D., Raftery, P., & Keane, M. (2014). A review of methods to match building energy simulation models to measured data. *Renewable and sustainable energy reviews*, *37*, 123-141.

Crawley, D. B., Pedersen, C. O., Lawrie, L. K., & Winkelmann, F. C. (2000). EnergyPlus: energy simulation program. *ASHRAE journal*, *42*(4), 49.

De Mets, T., Tilmans, A., & Loncour, X. (2017). Hygrothermal assessment of internal insulation systems of brick walls through numerical simulation and full-scale laboratory testing. *Energy Procedia*, *132*, 753-758.

De Wit, S., & Augenbroe, G. (2002). Analysis of uncertainty in building design evaluations and its implications. *Energy and Buildings*, *34*(9), 951-958.

Dhariwal, J., & Banerjee, R. (2015). Naturally Ventilated Building Design under Uncertainty Using Design of Experiments. Building Simulation Conference, 1708–1715.

Eisenhower, B., O'Neill, Z., Fonoberov, V. A., & Mezić, I. (2012). Uncertainty and sensitivity decomposition of building energy models. *Journal of Building Performance Simulation*, *5*(3), 171-184.

Erhorn, H., Erhorn-Kluttig, H., Thomsen, K. E., Rose, J., & Aggerholm, S. (2010). An effective Handling of Thermal Bridges in the EPBD Context: Final report of the IEE ASIEPI work on thermal bridges.

Finken, G. R., Bjarløv, S. P., & Peuhkuri, R. H. (2016). Effect of façade impregnation on feasibility of capillary active thermal internal insulation for a historic dormitory–A hygrothermal simulation study. *Construction and Building Materials*, *113*, 202-214.

Gao, X., & Malkawi, A. (2014). A new methodology for building energy performance benchmarking: An approach based on intelligent clustering algorithm. *Energy and Buildings*, *84*, 607-616.

Ge, H., McClung, V. R., & Zhang, S. (2013). Impact of balcony thermal bridges on the overall thermal performance of multi-unit residential buildings: A case study. *Energy and Buildings*, *60*, 163-173.

Guerra-Santin, O., & Itard, L. (2010). Occupants' behaviour: determinants and effects on residential heating consumption. *Building Research & Information*, *38*(3), 318-338.

Hachem, C. & Elsayed, M. (2016). Patterns of façade system design for enhanced energy performance of multistory buildings. *Energy and Buildings*, *130*, 366-377.

Hamza, N. (2008). Double versus single skin facades in hot arid areas. *Energy and buildings*, *40*(3), 240-248.

Helton, J. C., & Davis, F. J. (2003). Latin hypercube sampling and the propagation of uncertainty in analyses of complex systems. *Reliability Engineering & System Safety*, *81*(1), 23-69.

Hopfe, C. J. (2009). Uncertainty and sensitivity analysis in building performance simulation for decision support and design optimization. *PhD diss., Eindhoven University*.

Hopfe, C. J., & Hensen, J. L. (2011). Uncertainty analysis in building performance simulation for design support. *Energy and Buildings*, *43*(10), 2798-2805.

Hopfe, C., Hensen, J., & Plokker, W. (2007, September). Uncertainty and sensitivity analysis for detailed design support. In *Proceedings of the 10th IBPSA building simulation conference* (pp. 3-5). Tsinghua University.

Iommi, M. (2018). The mediterranean smart adaptive wall. An experimental design of a smart and adaptive facade module for the mediterranean climate. *Energy and Buildings*, *158*, 1450-1460.

Jain, A. K., & Dubes, R. C. (1988). Algorithms for clustering data.

Kaka, V. B. and Chao, S.-H. (2018). Investigation of Eliminating Prestress in Bridge Girders with the Use of Non-Prestressed Ultra-High-Performance Fiber-Reinforced Concrete Girders. ASCE Structures Congress. Fort Worth TX.

Karasu, A. (2015). Building energy efficiency with climate envelopes. *Contemporary Trends in the Regenerative and Sustainable Built Environment: Technical and Managerial Aspects*, 115.

Kashani, H., Ashuri, B., Shahandashti, S. M., & Lu, J. (2014). Investment valuation model for renewable energy systems in buildings. *Journal of Construction Engineering and Management*, *141*(2), 04014074.

Kashani, H., Ashuri, B., Lu, J., & Shahandashti, M. (2012). A real options model to evaluate investments in photovoltaic (PV) systems. In *Construction Research Congress 2012: Construction Challenges in a Flat World* (pp. 1641-1650).

Kotsiantis, S., & Pintelas, P. (2004). Recent advances in clustering: A brief survey. *WSEAS Transactions on Information Science and Applications*, *1*(1), 73-81.

Künzel, H. M., & Kiessl, K. (1996). Calculation of heat and moisture transfer in exposed building components. *International Journal of heat and mass transfer*, *40*(1), 159-167.

Lai, S. T., & Leu, F. Y. (2016, November). Data Preprocessing Quality Management Procedure for Improving Big Data Applications Efficiency and Practicality. In *International Conference on Broadband and Wireless Computing, Communication and Applications* (pp. 731-738). Springer, Cham.

Lam, J. C., Wan, K. K., & Yang, L. (2008). Sensitivity analysis and energy conservation measures implications. *Energy Conversion and Management*, *49*(11), 3170-3177.

Lechner, N. (2014). Heating, Cooling, Lighting: Sustainable Design Methods for Architects, 4th Ed., John Wiley & Sons, 2014.

Lee, B. D., Sun, Y., Augenbroe, G., & Paredis, C. J. (2013, August). Towards better prediction of building performance: a workbench to analyze uncertainty in building simulation. In *13th International Building Performance Simulation Association Conference, Chambéry, France*.

Li, Q., Gu, L., Augenbroe, G., Wu, C., & Brown, J. (2015). A Generic Approach to Calibrate Building Energy Models under Uncertainty Using Bayesian Inference. BS2015: 14th Conference of International Building Performance Simulation Association (pp. 2913-2922). Hyderabad, India.

Lomas, K. J, & Eppel, H. (1992). Sensitivity analysis techniques for building thermal analysis simulation program. *Energy and Buildings*, 19(1), 21–44.

Losch, E. D., Hynes, P. W., Andrews Jr, R., Browning, R., Cardone, P., Devalapura, R., & Kourajian, P. (2011). State of the art of precast/prestressed concrete sandwich wall panels. PCI Journal, 56(2), 131-176.

Lu, J., Ashuri, B., & Shahandashti, M. (2014). A data envelopment analysis model for building energy efficiency benchmarking. In *Construction Research Congress 2014: Construction in a Global Network* (pp. 1073-1082).

Macdonald, I., & Strachan, P. (2001). Practical application of uncertainty analysis. *Energy and Buildings*, *33*(3), 219-227.

Macdonald, I. A. (2002). *Quantifying the effects of uncertainty in building simulation* (Doctoral dissertation, University of Strathclyde).

Maliki, M., Laredj, N., Bendani, K., & Missoum, H. (2017). Two-dimensional transient modeling of energy and mass transfer in porous building components using COMSOL Multiphysics. *J. Appl. Fluid Mech*, *10*, 319-328.

McKay, M. D., Beckman, R. J., & Conover, W. J. (1979). Comparison of three methods for selecting values of input variables in the analysis of output from a computer code. Technometrics, 21(2), 239-245.

McKay, M. D., Beckman, R. J., & Conover, W. J. (2000). A comparison of three methods for selecting values of input variables in the analysis of output from a computer code. *Technometrics*, *42*(1), 55-61.

Menberg, K., Heo, Y., Augenbroe, G., & Choudhary, R. (2016). New extension of Morris method for sensitivity analysis of building energy models. *Building Simulation & Optimization 2016*.

Mitchell, R., Kohler, C., Arasteh, D., Carmody, J., Huizenga, C., & Curcija, D. (2003). THERM 5/WINDOW 5 NFRC simulation manual.

Moon, H. J. (2005). Assessing mold risks in buildings under uncertainty (Doctoral dissertation, Georgia Institute of Technology).

Mukhopadhyaya, P., Kumaran, K., Tariku, F., & van Reenen, D. (2006). Application of hygrothermal modeling tool to assess moisture response of exterior walls. *Journal of architectural engineering*, *12*(4), 178-186.

Multiphysics, COMSOL (2013). Comsol Multiphysics reference manual. *COMSOL: Grenoble, France*, 1084.

National Renewable Energy Laboratory. (1993). Solar and Meteorological Surface Observation Network 1961–1990, Version 1.0.

National Renewable Energy Laboratory. (2011). U.S. Department of Energy Commercial Reference Building Models of the National Building Stock. National Renewable Energy Laboratory.

Neto, A. H., & Fiorelli, F. A. S. (2008). Comparison between detailed model simulation and artificial neural network for forecasting building energy consumption. *Energy and Buildings*, *40*(12), 2169-2176.

Nikolaou, T. G., Kolokotsa, D. S., Stavrakakis, G. S., & Skias, I. D. (2012). On the application of clustering techniques for office buildings' energy and thermal comfort classification. *IEEE Transactions on Smart Grid*, *3*(4), 2196-2210.

Noël, J. A., Kahwaji, S., Desgrosseilliers, L., Groulx, D., & White, M. A. (2016). Phase change materials. In *Storing Energy* (pp. 249-272). Elsevier.

Ojanen, T., Viitanen, H., Peuhkuri, R., Lähdesmäki, K., Vinha, J., & Salminen, K. (2010). Mold growth modeling of building structures using sensitivity classes of materials. *Proceedings Buildings XI, Florida*.

Orlandic, R., Lai, Y., & Yee, W. G. (2005, October). Clustering high-dimensional data using an efficient and effective data space reduction. In *Proceedings of the 14th ACM international conference on Information and knowledge management* (pp. 201-208). ACM.

Parent, M. (2002) "Estimation du potentiel technico-économique d'économie d'énergie au Québec: Secteur commercial et institutionnel au tarif L" Québec, Rapport de Technosim Inc. pour Hydro-Québec.

Park, B., Srubar, W. V., & Krarti, M. (2015). Energy performance analysis of variable thermal resistance envelopes in residential buildings. *Energy and Buildings*, *103*, 317-325.

Pavlík, Z., & Černý, R. (2009). Hygrothermal performance study of an innovative interior thermal insulation system. *Applied Thermal Engineering*, *29*(10), 1941-1946.

Petr, K., Filip, J., Karel, K., & Jan, H. (2007). Technique of Uncertainty and Sensitivity Analysis for Sustainable Building Energy Systems Performance

Calculations. In *Proceedings of the 10th Conference of International Building Performance Simulation Association* (pp. 629-636).

Pramudiono, I., & Kitsuregawa, M. (2003, April). Parallel FP-growth on PC cluster. In *Pacific-Asia Conference on Knowledge Discovery and Data Mining* (pp. 467-473). Springer, Berlin, Heidelberg.

Pudasaini, B., Shahandashti, S. M., & Razavi, M. Identifying Critical Links in Water Supply Systems Subject to Various Earthquakes to Support Inspection and Renewal Decision Making. In *Computing in Civil Engineering 2017* (pp. 231-238).

Pudasaini, B., & Shahandashti, S. M. (2018). Identification of Critical Pipes for Proactive Resource-Constrained Seismic Rehabilitation of Water Pipe Networks. *Journal of Infrastructure Systems*, *24*(4), 04018024.

Real, S., Gomes, M. G., Rodrigues, A. M., & Bogas, J. A. (2016). Contribution of structural lightweight aggregate concrete to the reduction of thermal bridging effect in buildings. *Construction and Building Materials*, *121*, 460-470.

Rollins, S., & Banerjee, N. (2014, March). Using rule mining to understand appliance energy consumption patterns. In *Pervasive Computing and Communications (PerCom), 2014 IEEE International Conference on* (pp. 29-37). IEEE.

Roppel, P., Lawton, M., & Norris, N. (2012). Thermal Performance of Building Envelope Details for Mid-and High-Rise Buildings. *ASHRAE Transactions*, *118*(2).

Roth, M. (2017). Updating the ASHRAE Climate Design Data for 2017. *ASHRAE Transactions*, *123*.

Sadineni, S. B., Madala, S., & Boehm, R. F. (2011). Passive building energy savings: A review of building envelope components. *Renewable and Sustainable Energy Reviews*, *15*(8), 3617-3631.

Sailor, D. J. (2008). A green roof model for building energy simulation programs. *Energy and buildings*, *40*(8), 1466-1478.

Salleb-Aouissi, A., Vrain, C., & Nortet, C. (2007, January). QuantMiner: A Genetic Algorithm for Mining Quantitative Association Rules. In IJCAI (Vol. 7, pp. 1035-1040).

Salleb-Aouissi, A., Vrain, C., Nortet, C., Kong, X., Rathod, V., & Cassard, D. (2013). QuantMiner for mining quantitative association rules. The Journal of Machine Learning Research, 14(1), 3153-3157.

Shahandashti, S. M., Abediniangerabi, B., Bell, B., & Chao, S. H. Probabilistic Building Energy Performance Analysis of Ultra-High-Performance Fiber-

Reinforced Concrete (UHP-FRC) Façade System. In *Computing in Civil Engineering 2017* (pp. 223-230).

Shahandashti, S. M., & Pudasaini, B. (2019). Proactive Seismic Rehabilitation Decision-Making for Water Pipe Networks Using Simulated Annealing. *Natural Hazards Review*, *20*(2), 04019003.

Soleimani, M., & Shahandashti, M. (2017). Comparative process-based life-cycle assessment of bioconcrete and conventional concrete. Journal of Engineering, Design and Technology, 15(5), 667-688.

Soto, A. M., & Jentsch, M. F. (2015, December). Sensitivity and uncertainty analysis of models for determining energy consumption in the residential sector. In *Proceedings of BS2015: 14th Conference of International Building Performance Simulation Association, Hyderabad, India*.

Steeman, H. J., Janssens, A., Carmeliet, J., & De Paepe, M. (2009). Modelling indoor air and hygrothermal wall interaction in building simulation: Comparison between CFD and a well-mixed zonal model. *Building and environment*, *44*(3), 572-583.

Sun, Y., Heo, Y., Xie, H., Tan, M., Wu, J., & Augenbroe, G. (2011, November). Uncertainty quantification of microclimate variables in building energy simulation. In *12th International Building Performance Simulation Association Conference, Sydney, Australia*.

TenWolde, A. (2001). Manual analysis tools. *Moisture Analysis and Condensation Control in Building Envelopes. H. Trechsel. West Conshohocken, ASTM*.

Thalfeldt, M., Pikas, E., Kurnitski, J., & Voll, H. (2013). Facade design principles for nearly zero energy buildings in a cold climate. *Energy and Buildings*, *67*, 309-321.

Theodosiou, T. G., & Papadopoulos, A. M. (2008). The impact of thermal bridges on the energy demand of buildings with double brick wall constructions. *Energy and Buildings*, *40*(11), 2083-2089.

Theodosiou, T., Tsikaloudaki, K., & Bikas, D. (2017). Analysis of the thermal bridging effect on ventilated facades. *Procedia environmental sciences*, *38*, 397-404.

Tsanas, A., & Xifara, A. (2012). Accurate quantitative estimation of energy performance of residential buildings using statistical machine learning tools. *Energy and Buildings*, *49*, 560-567.

U.S. Department of Energy, Energy Efficiency & Renewable Energy Office. (2016a, August 08). Commercial Prototype Building Models. Retrieved from: https://www.energycodes.gov/development/commercial/prototype_models

U.S. Department of Energy, Building Technologies Office. (2016b, August 08). EnergyPlus. Retrieved from https://energyplus.net/.

U.S. Department of Energy, Energy Efficiency & Renewable Energy. (2018, February 27). Climate Zones. Retrieved from: https://energy.gov/eere/buildings/climate-zones.

U.S. Energy Information Administration. (2015 August 08). Link: http://www.eia.gov/tools/faqs/faq.cfm?id=86&t=1, Last visited: 12/12/16.

Vereecken, E., Van Gelder, L., Janssen, H., & Roels, S. (2015). Interior insulation for wall retrofitting–A probabilistic analysis of energy savings and hygrothermal risks. *Energy and Buildings*, *89*, 231-244.

Wagstaff, K., Cardie, C., Rogers, S., & Schrödl, S. (2001, June). Constrained k-means clustering with background knowledge. In *ICML* (Vol. 1, pp. 577-584).

Wang, L., Mathew, P., & Pang, X. (2012). Uncertainties in energy consumption introduced by building operations and weather for a the medium-size office building. *Energy and Buildings*, *53*, 152-158.

Xiao, F., & Fan, C. (2014). Data mining in building automation system for improving building operational performance. *Energy and Buildings*, *75*, 109-118.

Zhao, H. X., & Magoulès, F. (2012). A review on the prediction of building energy consumption. *Renewable and Sustainable Energy Reviews*, *16*(6), 3586-3592.

Zirkelbach, D., Schmidt, T., Kehrer, M., & Künzel, H. M. (2007). Wufi® Pro–Manual. *Fraunhofer Institute*.